ISTANBUL TECHNICAL UNIVERSITY ★ GRADUATE SCHOOL OF SCIENCE, ENGINEERING AND TECHNOLOGY

DESIGN, FABRICATION AND CHARACTERIZATION OF NANO-SI COLUMNAR STRUCTURES FOR SOLAR CELL APPLICATIONS

M.Sc. THESIS

Aysegul DEVELIOGLU
(513121001)

Department of Nanoscience and Nanoengineering

Nanoscience and Nanoengineering Programme

Thesis Advisor: Prof. Dr. Levent TRABZON

DECEMBER 2015

İSTANBUL TEKNİK ÜNİVERSİTESİ ★ FEN BİLİMLERİ ENSTİTÜSÜ

NANO-Sİ KOLON YAPILARININ GÜNEŞ PİLİ UYGULAMALARI İÇİN TASARLANIP, ÜRETİLİP, KARAKTERİZE EDİLMESİ

YÜKSEK LİSANS TEZİ

Aysegul DEVELIOGLU
(513121001)

Nanobilim ve Nanomühendislik Anabilim Dalı

Nanobilim ve Nanomühendislik Yüksek Lisans Programı

Tez Danışmanı: Prof. Dr. Levent TRABZON

ARALIK 2015

Aysegul DEVELIOGLU, a M.Sc. student of ITU Graduate School of Science Engineering and Technology student ID 513121001, succefully defended the thesis "Design, Fabrication and Characterization of n-Si Columnar Structures for Solar Cell Applications ", which she prepared after fulfilling the requirements specified in the associated legislation, before the jury whose signatures are below.

Thesis Advisor :	**Prof. Dr. Levent TRABZON** Istanbul Technical University	.....

Jüri Üyeleri :	**Prof. Dr. Levent Trabzon** Istanbul Technical University	.....
	Assoc. Prof. Huseyin KIZIL Istanbul Technical University	.....
	Prof. Dr. Haluk KUCUK Marmara University	.....

Date of Submission : NOVEMBER 22, 2015
Date of Defense : DECEMBER 29, 2015

To my family,

FOREWORD

Firstly, I would like to express my gratitude to my advisor Prof. Dr. Levent TRABZON for sharing his valuable experiences, his guidance and supoort during my research. Also I would like to thank all members of ITU MEMS and Nanotechnology Research Center. I would also express my gratitude to Muhammed BEKIN for valuable personal, scientific and technical support through my research.

I must also thank to Amin TABATABAEI MOHSENI for his generous help at the essential part of my research.

I would like to thank my family and my beloved friend Muhsin KAYMAKCI for their moral support.

I would like to thank to The Scientific and Technological Research Council of Turkey (TUBITAK) for supporting my thesis within priority areas scholarship.

December 2015

Aysegul DEVELIOGLU
(Physicist)

CONTENTS

Page

ABBREVIATIONS

Ag	**:** Silver
Al	**:** Aluminium
AM	**:** Air Mass
C	**:** Carbon
CdTe	**:** Cadmium Telluride
CIGS	**:** Copper Indium Gallium Selenide
CNT	**:** Carbon Nano Tube
CVD	**:** Chemical Vapor Deposition
CZTS	**:** Copper Zink Tin Sulfide
DC	**:** Direct Current
eV	**:** Electron Volt
FF	**:** Fill Factor
Ga	**:** Gallium
GLAD	**:** Glancing Angle Deposition
GW	**:** Giga Watts
I	**:** Current
In	**:** Indium
ITO	**:** Indium Tin Oxide
kW	**:** Kilo Watts
MPP	**:** Maxiumum Power Point
MW	**:** Mega Watts
NW	**:** Nanowire
P3HT	**:** Poly(3-hexylthiophene-2,5-diyl)
PCE	**:** Power Conversion Efficiency
PEDOT:PSS	**:** Poly(3,4-ethylenedioxythiophene)-poly(styrenesulfonate)
PV	**:** Photovoltaics
PVD	**:** Physical Vapor Deposition
QD	**:** Quantum Dot
rpm	**:** Revolutions Per Minute
SEM	**:** Scanning Electron Microscope
Si	**:** Silicon
STF	**:** Structured Thin Films
Ta	**:** Tantalum
TMB	**:** Trimethyl Boron
V	**:** Volt
W	**:** Tungsten

LIST OF SYMBOLS

c	**:** Speed of light
E	**:** Illumination
h	**:** Planck's constant
n	**:** Electron concentration
$\mathbf{N_A}$	**:** Acceptor atom concentration
p	**:** Hole concentration
r	**:** Radius
W	**:** Energy
η	**:** Power conversion efficiency
λ	**:** Wavelength
ν	**:** Frequency
π	**:** pi number

LIST OF TABLES

Page

LIST OF FIGURES

Page

DESIGN, FABRICATION AND CHARACTERIZATION OF N-SI COLUMNAR STRUCTURES FOR SOLAR CELL APPLICATIONS

SUMMARY

Energy demand has had an increasing growth since industrial revolution at the end of the 19th century. One reason for growth of energy demand is incresing world population. It has doubled in last 40 years. The second reasons is rising in life standarts. Generation, transmission and distribution of electricity were considered as a strategic management for a lot of country. However nuclear accidents in Chernobyl and Fukushima, global raming problem and carbon emission, direct a lot of countries to the renewable energy sources. Germany is the leader country in solar energy investments and has a national target to obtain 50% of its energy consumption from renewable energy sources. Investments and researches have been increasing in this field in last two decades due to the abundance of silicon in the nature, sun is an infinite source, less cost and less material consumption through cutting-edge material deposition techniques.

Solar cells contain p-n junction which can be conceived as two type of semiconductors have a surface in common. In this system majority careers in n type (electrons) begin to diffuse into p region and recombine with holes. Similarly, majority careers from p type semiconductor (holes) begin to diffuse into n region and recombine with electrons. Therefore depletion layer, where no charge careers exist, occured near the junction. When this system expose to the light minority careers from both sides cross through depletion zone and generete a current.

First generation solar cells are based on simple p-n junction. The second generation cells are made of doped thin films typically Cadmium Telluride (CdTe), Copper Indium Gallium Selenide (CIGS), Copper Zink Tin Sulfide (CZTS). These materials have ideal bandgap for solar cells however their scarcity and cost limit the use. The third generation solar cells are made of quantum dots. QDs are semiconductor particles and their bandgap can be tunable. Through this property this structures are able to harvest wide range of solar radiation. The fourth generation of solar cells are based on hybrid inorganic crystals within polymer molecules.

In this thesis n type amorphous silicon columnar structures were deposited through glancing angle deposition technique in different geometries. Cross-sectional and top-view SEM images show that these structures have more porous structures compared to flat surface. As a result of this colomnar structures possess less reflectivity according to the UV-VIS spectroscopy which means these structures absorb more photons compred to flat surface. This is an important factor to increase efficiency of solar cells by increasing light trapping.

Porous surface have also changed the surface hydrophobisity. According to the contact angle measurements flat silicon have 98^{o} while columnar structures have 71^{o}

and 61°. This is important both for increase light trapping and better distribution of PEDOT:PSS hole conductor polymer layer on the surface.

AFM images scanned in 1μmx1μm area also shows that columnar structures exhibit more surface roughness compared to flat surfaces.

PEDOT:PSS was covered using spin coating method. First it was dropped onto surface and wait for 1min. then it was spin coated with 2000rpm twice. UV-VIS spectroscopy shows that PEDOT:PSS is highly transparent and suitable for solar cell applications. Also SEM images of PEDOT covered silicon structures show that columnar structures have larger p-n junction interface area due to both porous surface and hydrobilicty.

Another method to increase efficiency of such structures is to create different geometries by different methods such as chemical vapor deposition and etching to increase surface porosity. We can also use mono-crystalline materials instead of poly-crystalline and amorphous materials to prevent dangling bonds which can cause current leakage. Also surface treatment techniques such as oxidation and hydrogen terminating can be apply to the absorber layer surface. For bottom up methods cooling down the substrate provides better distrubution of columnar structures. Quantum dots and carbon nanotubes can be added to absorber layer to reduce reflectivity and increase absorption. Some chemicals can be added to PEDOT:PSS polymer to increase hole concentration.

NANO-SI KOLONSAL YAPILARIN GÜNEŞ PİLİ UYGULAMALARI İÇİN TASARLANIP, ÜRETİLİP, KARAKTERİZE EDİLMESİ

ÖZET

Enerji ihtiyacı 19. yüzyılda sanayileşme ile birlikte artmaya başlamış ve günümüzde küresel bir sorun halini almıştır. Bunun başlıca nedenleri ise Dünya nüfsunun son 40 yıl içersinde iki katına çıkması ve giderek artan yaşam standartlarıdır. Gelişmiş ve sanayileşmiş ülkelerde elektrik enerjisi üretimi, iletimi ve dağıtımı stratejik yönetim olarak kabul edilmektedir. Fakat son yıllarda yaşanan Chernobyl, Fukushima gibi nükleer felaketler, karbon salınımı ve sera gazlarının neden olduğu küresel ısınma bir çok ülkeyi elektrik enerjisi üretiminde yenilenebilir enerji kaynaklarına yöneltmiştir. Bu ülkelerin başında 2030 yılında enerji üretiminin %50sini yenilenebilir enerji kaynaklarından elde etmeyi planlayan Almanya gelmektedir. Almanya'nın ardından temiz enerjiye büyük oranda yatırım yapan diğer ülkeler arasında İtalya, 2011 yılında yaşadığı tsunami ve nükleer felaketten sonra enerji politikalarını büyük ölçüde değiştiren Japonya, ABD ve Çin başı çekmektedir. Güneş enerjisinin sonsuz bir enerji kaynağı olması, güneş pili üretiminde kullanılan silisyumun doğada bol bulunan ve temiz bir element olması, sadece %10 verimlilikle Sahra çölünde 700km^2 lik alana düşen güneş enerjisinin dünyanın ihtiyaçlarını karşılamaya yetecek olması ve nanoteknolojik malzeme ve yeni üretim teknolojileriyle verimliliğin arttırılıp fiyatların düşmesi hem akademik alanda hem sanayide bu alana milyar dolarlık yatırımlar yapılmasını sağlamıştır.

Güneş hücreleri genel olarak p ve n tip olmak üzere iki tip yarı iletkenin birleşmesinden oluşur. İki tür yarı iletkenin yüzeyleri bir araya geldiği zaman n tip yarı iletkende çoğunuk taşıyıcılar olan elektronlar arkasında bir "boşluk" bırakarak p tip yarı iletkene geçer ve burdaki pozitif değerlikteki "boşluk"larla birleşir. Aynı şekilde p tip yarı iletkendeki çoğunluk taşıyıcı olan pozitif yüklü "boşluk"lar da n tip yarıiletken tarafına geçerek burdaki negatif yülü elektronlarla birleşir ve deplesyon bölgesi denilen yüksüz bölgeyi oluştururlar. Bu durum iki yarıiltken bi araya geldiğinde kendiliğinden oluşan durumdur. Bu sistem bir ışığa yani foton uyarımına maruz kaldığında n tip yarı iletkendeki azınlık taşıyıcılar (boşluklar), p tip yarı iletkendeki azınlık taşıyıcılar (elektronlar) deplesyon bölgesinden karşı tarafa geçerek akım oluştururlar.

Ilk jenerasyon güneş pilleri temel olarak iki tip yarı iletkenin birleşiminden oluşmaktadır. İkinci jenerasyon piller Cadmium Telluride (CdTe), Copper Indium Gallium Selenide (CIGS), Copper Zink Tin Sulfide (CZTS) gibi katkılı malzemelerden oluşan ince filmleri (1 mikrondan daha ince katmanlar) içerir. Fakat bu malzemeler doğada kısıtlı sayıdadırlar. Üçüncü jenerasyon piller quantum dot temelli güneş pilleridir. Quantum dotlar boyutları değiştirilerek band aralığı değiştirebilen yarı ilekten parçacıklardır ve bu özellikleri de onları güneş pillerinde absorbe edilen radyasyon aralığını genşletme açısından ideal kılar. Son olarak

dördüncü jenerasyon piller hibrid inorganik kristaller ve organik yarı iletken polimer yapının birleşiminden oluşan güneş pilleridir.

Bu tezde güneş pili uygulamları için inorganik kristal olarak amorf yapıda n tip yarı iletken silisyum kullanılmış farklı geometrilerde üretilerek güneş pili verimliliğini etkileyen parametreleri incelenmiştir. Silisyum ince filmler fiziksel buhar depolama yöntemiyle düz filmler halinde ve açılı depolama yöntemi ile spiral, yatay, dik kolonsal olarak çeşitli geometrik yapılarda üretilmiş düz yüzeyle optik ve yapısal olarak karşılaştırmaları yapılmıştır. Organik yarı iletken olarak PEDOT:PSS seçilmiş ve güneş pili uygulamarı için geçirgenlik ölçümleri yapılmıştır.

Güneş pillerinde verimliliği arttırmanın en önemli faktörü p ve n tip yarı iletkenlerin arayüzey alanını arttırmaktır. Başka bir deyişle p ve n tip yarı iletkenler birbirlerine ne kadar çok temas ederlerde elektron ve "hole" üretimi o kadar fazla olur. Belirli bir kalınlıktan sonra malzemeler yük taşıyıcılar için bariyer oluşturacağından malzemeyi kalınlaştırmak yaklaşık 1 mikrondan sonra verimliliği arttırmayacak tam tersine düşürecektir. Silisyum için optimum aralık 300-800nm arasındadır. Bu nedenle önemli olan farklı tasarım ve geometrilerle p-n ekleminin arayüzeyini arttırmaktır.

Güneş pili verimliliğinde ikinci önemli faktör ışığı emici malzemenin yansımasını düşürerek daha fazla foton absorbe etmesini sağlamak böylece daha fazla elektron ve "hole" üretimi elde etmek. Işık emici yüzey ne kadar ışık tutarsa sistemin verimliliği o kadar fazla olacaktır.

Dördüncü jenerasyon güneş pillerinde başka bir önemli faktör yüzeyin su severliğidir. Silisyum normal şartlarda hidrofobik bir karaktere sahip olduğundan farklı geometrilerle ve yüzey porozitesiyle hidrofilikliği arttırılırsa organik polimer yüzeyde daha iyi bir şekilde yayılacak ve daha düzgün bir p-n eklemi oluşacaktır.

Son olarak güneş pili için dikkat edilebilecek önemli bir husus elektrod için kullanılacak malzemelerin seçimidir. Kontakt olarak kullanılacak iletken malzemelerin güneş pilinde kullanılan yarı iletkenlerle Schottky bariyeri oluşturmadığına dikkat edilmelidir. Elektrodlar ile yarı iletken malzemeler arasındaki bağlantı kayıp olmaması açısından Ohmic olmalıdır. Silisyum ve polimer yarıiletkenler için en iyi elektrod malzemeleri Al, Ag ve Indium Tin Oxide (ITO)'dır.

Bu çalışmada yaklaşık 450nm silisyum düz yüzey, 80^o açı ile tutularak eğik kolonsal yapılar ve 80^o ile 25rpm hızla döndürülerek dikey kolonsal yapılar fiziksel buhar depolama yöntemi ile yaklaşık 10^{-7} Pascal basınç altında 1 Å/s depolama hızıyla elde edilmiştir. Örneklerin kesit ve üsy yüzeylerinin elektron mikrsokopu görüntüleri alınmış kolonsal yapıların üst yüzeylerinin düz filmden çok daha poruslu olduğu görülmüştür.

UV-VIS spektroskopisinde yapılan ölçümlerle kolonsal yüzeylerin yansımasının düz yüzeyden çok daha az olduğu tesbit edilmiştir ki bu da güneş pili verimliliğinde ışık emici yüzey için verimliliği arttıracak önemli bir faktördür. Düz yüzetin yansıması 0.8-0.9 civarında iken kolonsal yüzeylerin yansımaları 0.5 ve 0.3 aralığındadır ki düşen yansıma değeri foton absorbansını arttırmaktadır.

Örneklerin su ile temas açısı ölçümleri yapılmış silisyum düz yüzeyin temas açısı ortalama 95^o iken kolonsal yapıların temas açılarının ortalama 60^o olduğu görülmüştür. Poruslu yüzey yapısı silisyumun hidrofobikliğini azaltmıştır. Bu da hibrid güneş pilleri için önemli olan polimer yüzeyin silisyumla daha iyi bir p-n eklemi oluşturmasını sağlamaktadır.

Örneklerin XRD ölçümleri yapılmış fakat amorf yapılar kullanıldığından dolayı pik gözlemlenmemiştir.

Çalışmada organik polimer olarak kullanılan PEDOT:PSS spinner ile yüzeye kaplanmıştır. Parçacıklı yapısı nedeniyle 45mikronluk süzgeçten geçirilmiş yüzeye damlatılıp 1dk beklendikten sonra 2000rpm hızda iki kere döndürülerek yüzeye kaplanmıştır. Alınan kesit SEM görüntülerinde görülmüştür ki PEDOT:PSS kolonsal yüzeylerde hem yüzeyin su severliği nedeniyle daha iyi yayılmış hem de poruslu yapısı nedeniyle daha geniş bir p-n eklemi oluşturmuştur. Düz yüzeylerde ise yüzeyin hidrofobikliği nedeniyle homojen bir dağılım ve geniş bir kesit alanı gözlenememiştir. Kesit alanının genişliği ve yüzey hidrofilikliği güneş pili verimliliğini etkileyen en önemli faktörlerdendir.

Son olarak UV-VIS spektroskopisi ile PEDOT:PSS'in geçirgenliği incelenmiş ve geçirgenlik oldukça yüksek çıkmıştır. Bu da güneş ışınlarının polimerden geçerek silisyum absorbera ulaştığını göstermektedir.

Literatürde gerek fiziksel buhar depolama yöntemi ile gerek kimyasal depolama ve aşındırma yöntemleri ile elde edilen kolonsal yapıların düşük yansıması nedeniyle opto-elektronik cihazlarda verimliliği arttırıdığı hem silisyum hem diğer malzemler için görülmekte ayrıca bu tür yapılar elektro-kimyasal olarak sentezlenmiş güneş pillerinde verimliliği arttırmak amacıyla "anti-reflection coating" olarak kullanıldığı görülmüştür. Bu tür yapılar aynı zamanda açık devre voltajı, kısa devre akımı, "fill factor" gibi fotovoltaik özelliklerin gelişmesine de yardımcı olmuştur.

Bu tip cihazların verimliliğini arttırmak için yapılabilecek diğer yöntemlerin başında amorf malzeme kullanmakar yerine "dangling bond"lardan kaynaklanan kayıpları önlemek amacıyla kristal malzeme kullanmak gelmektedir. Ayrıca oksitleme gibi yüzey iyileştirme yöntemleri de kullanılabilir. Kimyasal buhar depolama ve aşındırma yöntemiyle yüzey alanını ve poruslu yapıyı arttırmak amacıyla çeşitli tasarım ve geometride malzemler üretilebilir. Karbon nanotüp ve quantum dotlar kullanılarak emici yüzeylerin absorbansı arttırılabilir. "bottom-up" yöntemler için yüzeyi soğutmak kolonsal yapıların yüzeyde daha düzgün dağılmasını sağlayacağından daha homejen bir yapı elde edilebilir. Ayrıca çeşitli kimyasallarla (dimethyl sulfoxide, methoxyethanol) PEDOT:PSS yarı iletken polimerin "hole" konsantrasyonu arttırılabilir.

1. INTRODUCTION

Energy demand has had an exponential growth since the birth of industrial electricity at the end of the 19th century. At the beginning of 20th century building large electric power girds let many countries to bring the benefits of electricity to their citizens, while developing industrial applications of electricity. Today the growth use of electricity throughout the world in domestic applications made it major concern [1,2].

One reason for the growth of energy requirements is the growth of world population. It has almost doubled in last 40 years from 4 billion to 7.3 billion [3]. The second reason for this growth is the rising living standarts. The requirements of primary energy in Bangladesh, which is weak industrialized country, is 1500kWh/head while primary energy requirements in Germany is approximately 45 000kWh/head. With growing standarts in developing countries, requirements and consumption of primary energy increase substantially [4,5]. Figure 1.1 shows world marketed energy consumption by regions.

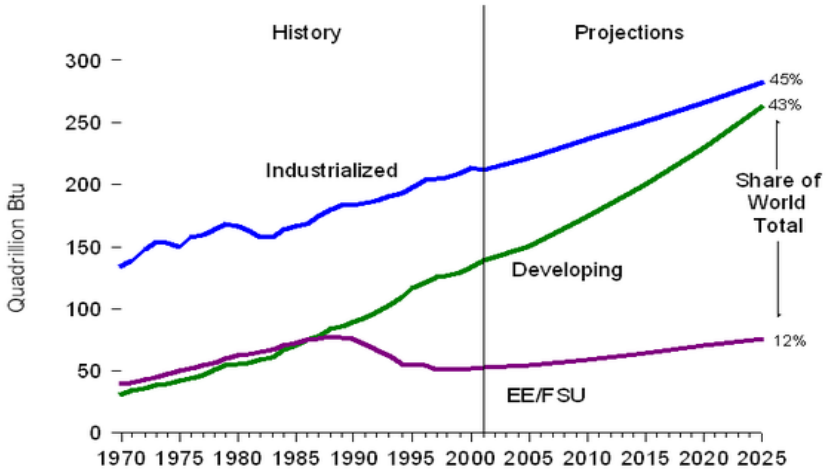

Figure 1.1: World marketed energy consumption by nations [6].

Generation, transmission and distribution of electricity were considered as a strategic management in many countries. However, electricity is an energy vector not an energy source. This means that we need to produce electric power by converting primary energy sources. One of the controversial methods is nuclear energy. Nuclear

power, or nuclear energy is the use of nuclear fission process to generate heat and electricity. Nuclear power stations provide about 13% of the world's electricity in 2012. According to IAEA 2015 there are 439 nuclear power plant in 31 countries with a net capacity of 377 gigawatts GW. 69 plants are under construction [7,8]. Hydroelectric power is one of the oldest technique of producing power. Hydroelectricity is the term referring to electricity generated by hydropower. Electricity is generated using gravitational force of falling or flowing water. Hydropower provides 19% of total electricity production [9]. Geothermal energy is a thermal energy generated and stored in the Earth. Earth's internal heat is a thermal energy comes from radioactive decay and there is continuous heat loss since Earth's formation. Earth's thermal energy has been used for electricity generation and produces 11.400 megawatts (MW) in 24 countries [10]. Geothermal power is reliable, cost-effective, sustainable and environmental friendly but limited to certain hot, tectonic areas. Fossil fuels such as coal, natural gas and petroleum are burnt to produce electricity.Coal-fired power plants provide 46% of consumed electricity in United States however they are major emitter of CO_2 and causes global warming [11]. Also fossil fuels are non-renewable and un-sustanable resources and will eventually become exhausted. People have been harnessing wind's energy for hundreds of years. Wind exists because sun cannot heat Earth's ground evenly. Hot air rises and cooler air move down to fill the gap. Wind flow or energy is harvested by modern wind turbines that can be as tall as 20 – story building and have three 60 – meter – long blades [12]. The wind spins the blades, generator receives mechanical energy and converts it into electricity and then electricity is transmitted to the utility grid. Wind is a clean source of renewable energy and produces no pollution and greenhouse gases. Since the wind is free operational cost is too low and advanced technology is making wind turbines cheaper and more efficient. In Europe, Germany and Spain are leading with 39.165 MW and 22.987 MW installed wind power capacity, respectively, China has 114.763 MW and U.S.A has 65.879 MW installed wind power capacity at the end of the 2014 [13]. In 2014, wind power provided 41.2% of Denmark's energy consumption [14]. Wind energy production is around 4% of total worldwide electricity usage and growing rapidly [15]. Figure 1.2 shoes the global annual installed wind capacity between 1997-2014 [13]. However there are some negative effects. Wind turbines can be deadly for birds around them and noise

genereted by wind turbines may be around 45 dB but after 1.6 km becomes inaudible.

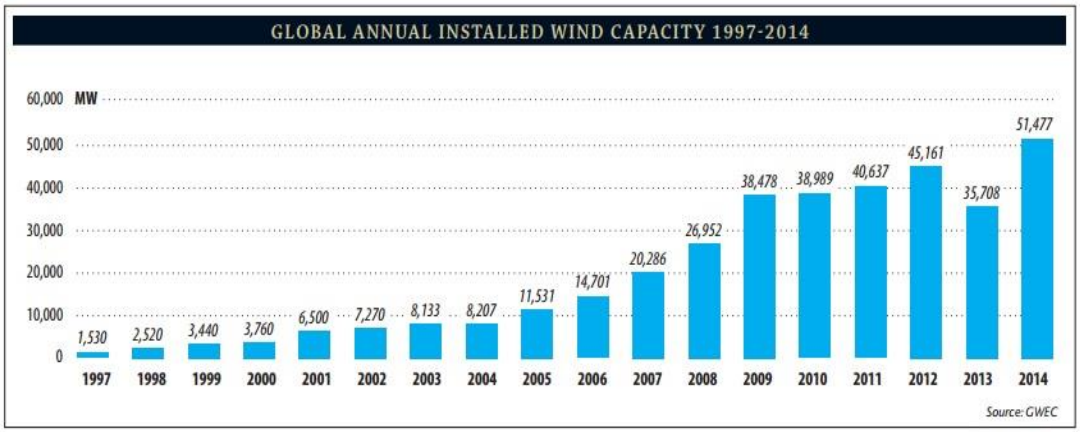

Figure 1.2 : Global Annual Installed Wind Capacity between 1997-2004.

The sun is our planet's main source of energy and an important source for renewable energy. Solar power is light and heat come from the sun and can be harnessed by solar thermal collector, photovoltaics, and solar panels. These systems absorb sunlight and convert it into electricity.

Inside the sun hydrogen atoms combine to make helium, and this process produce the extreme amount of heat that can be felt on Earth's surface. The core of the sun has a temperature of 36.000.000ºF (20.000.000ºC) and the surface has a temperature of 10.000ºF (5.538ºC) and the sun sends almost unimaginable amount of energy towards Earth – around 10^{17} (one hundred thousand million million watts) [16, 17]. However the majority of solar radiation falls on oceans. Also some is interrupted by clouds and arrives inconvenient places. About 70% of solar energy is absorbed by oceans and keep them from freezing. It also prevents Earth's atmosphere from freezing.

Solar technologies can be divided into two systems, passive solar and active solar. Passive solar energy systems capture the heat from the sun and use it without mechanical or electrical devices. People have been using solar energy this way since ancient times. Ancient Greeks, Romans and Chinese designed and placed their homes based on the principles of solar heating. Today passive solar systems focus on the maximize the potential of solar heating and cooling of homes and buildings. One important factor for passive solar design is "daylighting." Placement and design of windows is used to increase efficiency of natural sunlight inside the building.

Another type of passive solar system is solar collector which is relatively new technology made of dark metal. When sunlight hits a dark object, that object heats up. Solar collectors work based on this well known principle and heat buildings by heating air. They are also used to cool buildings in summertime [17]. Figure 1.3 shows a solar heater on the roof [18].

Figure 1.3 : A solar water heater sits on the roof in Greece.

Active solar systems are called as photovoltaic systems (PV). These systems use well known effect of physics: semi conductors convert light into electrical current. Photovoltaic systems are also called as solar cells that include thin layers of semiconductor material. Most commonly, these materials are silicon and cadmium telluride. These layers have tiny amount of doping agents. Doping agents are important because they give the semiconductor the ability of making electric current when expose the light. Germanium and boron are most frequently used doping agents. Each photovoltaic cell converts light into electricity with 5% to 20% efficiency.

Cells are often mounted in groups called modules. When PV modules put into together then they form an array. Figure 1.4 (a) shows the silicon cell module and array. These arrays can be used to make electricity for buildings. A 3.9 – inch (10 – centimeter) diameter PV cell can produce about one watt of power if the sun directly overhead and conditions are clear. If many arrays are combined they can create enough power to power a power plant [17]. Figure 1.4 (b) shows the power plant in

Arizona. Some concentration systems can also be used to increase power producing such as mirrors or lenses to focus sun light on PV cells.

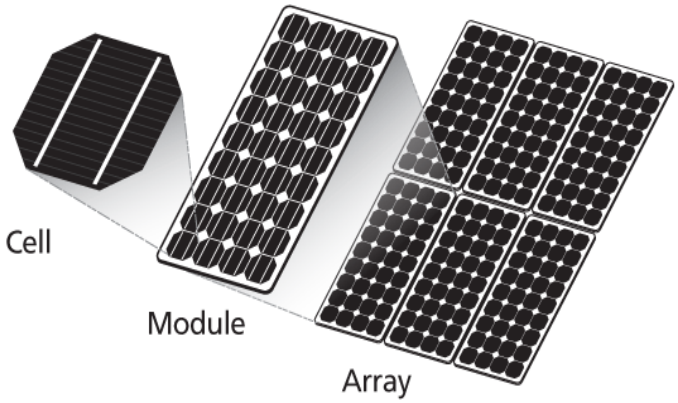

(a)

(b)

Figure 1.4 : (a) Silisium photovoltaic cell, module, array [19] (b) Solar PV power plant in Arizona [20].

1.1 Solar Economy, Policies and R&D Investments

Spending for research and development is necessary in early stages of development of new technologies. Germany is one of the leading countries in renewable energy investments. The country has a national target to reach 51 GW solar PV capacity by 2020. Germany has started serious of campaings to promote the use of renewable energy since 1986. In 2010 the National Renewable Energy Action Plan has projected to share renewable energy 38% by 2020, 50% by 2030, 65% by 2040 and 80% by 2050. Robert Bosch (RBOS), the world's biggest car supplier, has invested

about 1.5 billion Euros into its solar energy business. More than fifty institutes have researchs on PVs [21]. It has been seen that Germany has the biggest installation of solar PV cells during past decades. According to Reuters, Germany aims to reduce greenhouse gas emission by 40% and puts priority to promote renewable energy through government policies [22, 23]. Figure 1.5 shows a solar village in Germany.

Figure 1.5 : A solar city in Germany that prodeces four times energy it consumes [24].

Solar PV sector dominates in Italy's renewable energy sector because Italy has high solar radiation. Italy has aimed to reach 17% share of renewable energy by 2020. To achieve this aim, Italy has implemented some policies, such as green certificates, feed – in tariffs, market premiums to promote renewable energy sources. The Italian Government also introduced tax – based policy which allows the owners of solar PV installation on roof less than 20 kW capacity to deduct 30-50% of system capital expenditure [21].

Fukushima nuclear disaster has substantially changed the energy policies and politics of Japan. The government has taken the project for renewable energy generation. It will be 20% and 35% of total energy generation by 2030 and $700 billion will be invested. The Energy Policy Paper has been released by the Institute for Sustainable Energy Policies and presented long and short term energy strategy for installation of renewable energy by 100% of total power consumption. Japan generates solar PV power less than 1% of national consumption. The Japanese government also aimed that to reach capacity of 28 GW and 53 GW by the end of the 2020 and 2030, respectively. A banking firm, Japan Regenesis Trust announced that it has started operation of "Smart Farm" in Urakawa Town, Hokkaido [21].

In 2007, China established a "Medium and Long Term Development Plan for Renewable Energy in China" which aimed that consumption of energy from renewable sources would go up to 15% by 2020 and the two-third of the country receives solar radiation about 5020 MJ/m^2 and has annual sunshine about 2000 hour. China has given focus on province of Quinghai, Gansu, Ningxia, Xinjiang and Inner Mongolia which receive the highest solar radiation in the country. Also the Chinese government introduced "New FIT Regulation" schemes for development of large scale systems and as a result of this in 2012, Figure 1.6 shows that PV system prices had fallen 83.3% and 43% compared to the year of 2007 and 2011, respectively [21, 25].

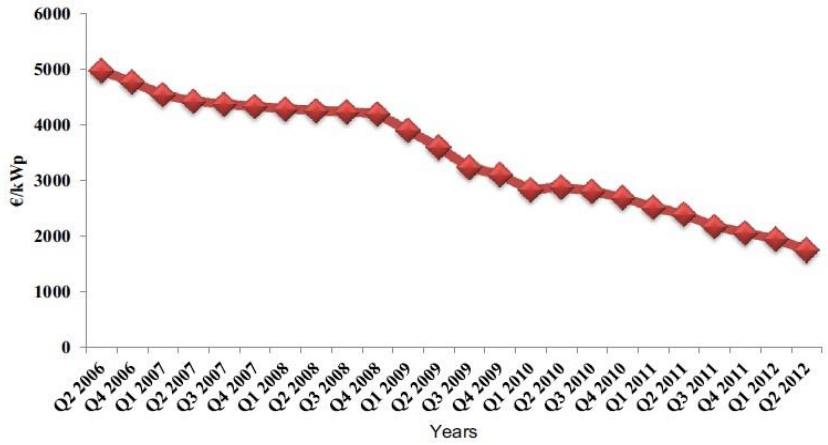

Figure 1.6 : PV price index – system price decreasing steadily [26].

The United States uses around 20% of all primary energy consumed worldwide [27]. In 2009-2010 USA shared 11% of total electricity from renewable energy sources and solar energy grew up by 77%. USA was leading country among the G-20 countries for the investments of clean energy. In 2012, USA reached 7.2 GW solar power capacity, at the state levels, California reached 1033 MW, followed by Arizona with 710 MW. The eleven states installed over 50 MW capacity of solar PV alone in 2012 [21, 28]. Figure 1.7 shows the solar PV installed capacity of top ten countries between 2007 and 2012 [21].

Apart from these policies and investments there is an intercontinental project name of *Desertec*. The basic idea was to take advantage of the enormous quantity of energy falling down on world's desert from the sun. An area of the Sahara 200 km by 200 km would suffice to cover current global energy consumption. If this sunlight could only be used with 10% efficiency, we would still only need an area 700 km by 700 km to provide our global energy consumption [29].

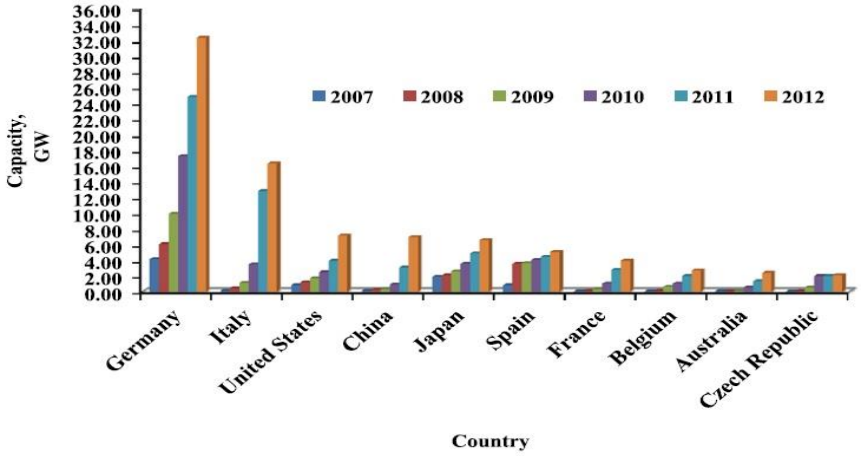

Figure 1.7 : Solar PV installed capacity of top ten countries between 2007 and 2012.

The concept of Desertec was developed by the Trans – Mediterranean Renewable Energy Cooperation (TREC) as a non – profit organization based in Germany. A few months later 12 companies created a consortium known as Desertec industrial initiative (Dii) to help push forward the project. The focus area of both organization was Europe, Middle East and South Africa (EU-MENA). As a part of project, it was intended to install a network of solar power system in the Saharan deserts of Morocco, Algeria, Jordan and Egypt. The project also contained high voltage direct current cables connecting MENA and EU. However, the project reached a dead end after several misfortunes. By mid – 2013, the Desertec Foundation and Dii split up, Dii failed to get support from Spanish government. Desistement of Spanish government made it impossible to transmit electricity from Morocco to Europe [30].

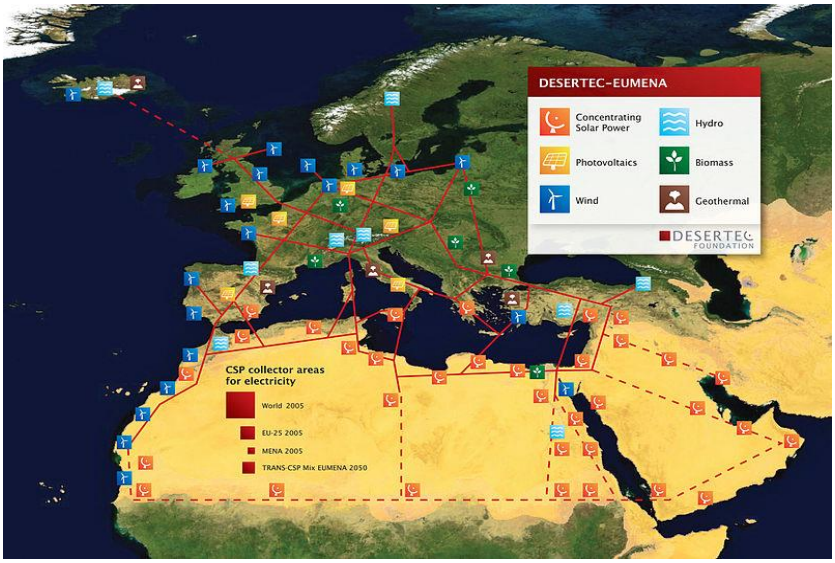

Figure 1.8 : Sketch of possible infrastructure for a sustainable supply of power to Europe, the Middle East and North Africa [31].

1.2 Why Nanoscience is Related to the Solar Industry

There are two key parameters for solar cell industry – cost and efficiency. Nanotechnology plays an important role in enhancing efficiency of solar cells. Nano-scaled materials are not only making solar cells more efficient, also making them cheaper to manufacture, easier to install and reducing thickness and size of some elements in a photovoltaic cells will save on materials. It is expected that nanotechnology has an impact on energy harvesting, production and storage on PV cells.

Solar cells can be classified into four generetions. First generation solar cells are based on simple p-n junction. They are generally made of n-type (phosphor doped) and p-type (boron doped) silisium and due to abundance of material still dominating the market share. Although Si is the most commonly used semi-conductor in solar industry there is a handicap. Si has indirect bandgap which means electrons in the valence band cannot transfer directly to the conduction band and this phenomena causes loses in light absorption.

Second generation solar cells are made of thin films (layers less than 1 micron) of Cadmium Telluride (CdTe), Copper Indium Gallium Selenide (CIGS), Copper Zink Tin Sulfide (CZTS). These materials have direct band gap and ideal for solar cell applications (1.1 and 1.7eV) but cost of them and their scarcity limit the use. Also amorphous and polycrystalline silicon are commonly used in thin film solar cells [32, 33]. Figure 1.9 shows the device structure of CdTe solar cell [34].

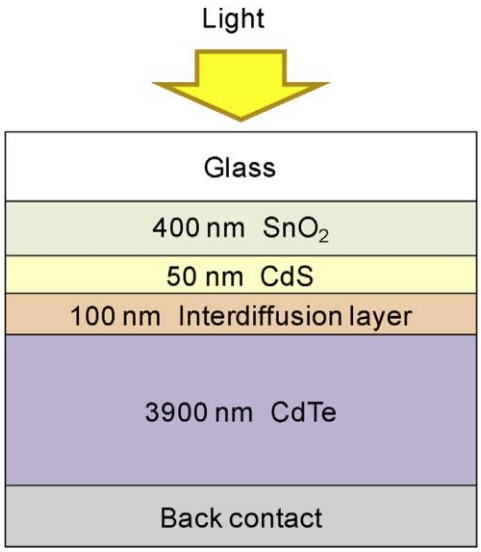

Figure 1.9: Device structure of CdTe solar cell.

Third generations are quantum dot based solar cells. Quantum dots are semiconducting particles and their bandgap is tunable by changing quantum dot's size. This ability makes quantum dots ideal for PV applications. Since the size and bandgap of QDs can be tunable in wide range, their solar cell applications can harvest wide range of solar radiation [35]. Figure 1.10 shows the cost-efficiency index of first, second and third generation solar cells [36].

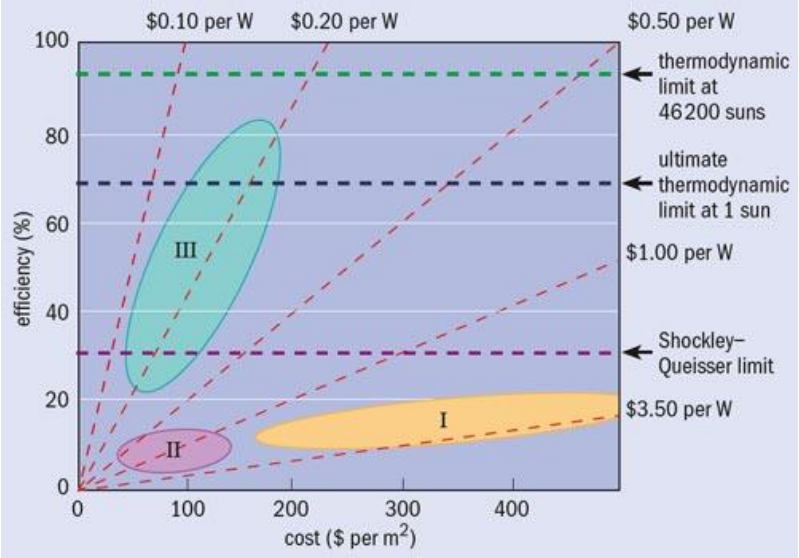

Figure 1.10 : Efficiency and cost projections for first, second and third generation PV technologies.

Fourth generation solar cells are based on hybrid-inorganic crystals within polymer molecules. Combination of organic (normally conjugated polymers) and inorganic compound aims that low cost of cell production and high power conversion efficiency (PCE). In such systems design of inorganic compound used as electron acceptor is very crucial. Electronic band structure of this material is also another important factor for high PCE. Typical acceptor materials for these kinds of systems are cadmium compounds, silicon, metal oxide nano particles and low bandgap nanoparticles. Solution processing of organic polymers is another factor that reduce the cost. These materials are Poly(3-hexylthiophene-2,5-diyl) (P3HT), Poly(3,4-ethylenedioxythiophene) (PEDOT:PSS), PCPDTBT:PCBM, MDMO:PPV and act as electron donor and hole transporter. Inorganic acceptor can be grown into desire shape onto substrate using different kinds of deposition techniques such as bottom-up and top-down processing and contact with the donor organic compound then back and top contacts are coated for electrical connection [37]. Figure 1.11 shows the development of publications in solar energy with nanotechnology [38].

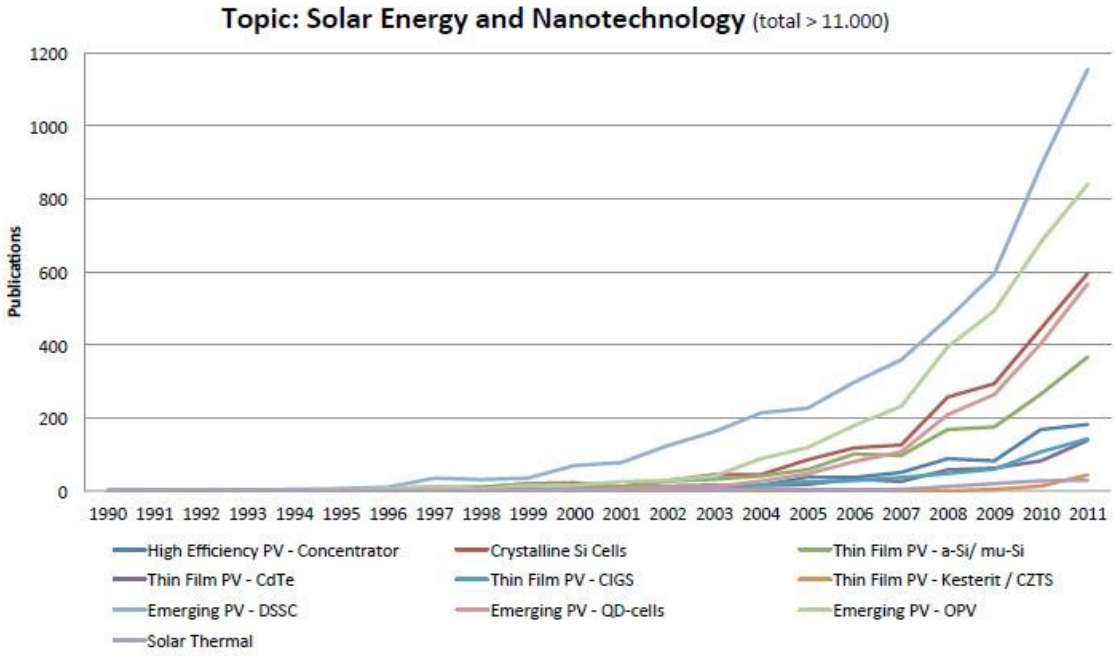

Figure 1.11 : Development of the number of publications in solar energy concerned with nanotechnology [38].

1.3 Purpose of Thesis

Reducing reflectivity is the important factor not for only solar cell for all optic devices to increase light absorbtion therefore efficincy and important photovoltaic parameters such as open circuit voltage, short sircut density and fill factor which means quality of solar cells. In this thesis design and fabrication of highly porous columnar structures have been aimed to reduced reflectivity by glancing angle deposition method for solar cell applications. Also increasing p-n junction interface area and reducing surface hydrophobicity of silicon absorber layer to increase light trapping and electron-hole generation are another purposes of this thesis.

1.4 Literature View

He *et al.*[39] fabricated Si nanowires by using electroless chemical etching method onto (100) n-type Si wafer. The etch times was varied to obtain nanowires with different lengths. Si nanowires with the lengths of 0.35, 0.9, 2.2, 4.1μm coated by PEDOT:PSS by using spin coater and 250-nm-thick aluminum and silver metal grid was coated by e-beam deposition as contact layers. Figure 1.12 shows the cross-sectional SEM images of SiNWs coated with PEDOT:PSS.

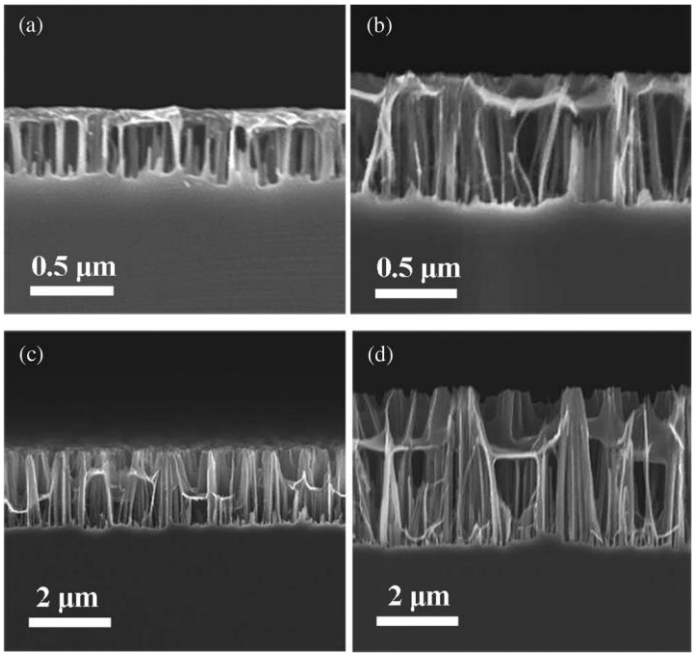

Figure 1.12: Cross-sectional SEM images of (a) 0.35, (b) 0.9, (c) 2.2 and (d) 4.4µm coated with PDEOT:PSS.

AM 1.5 solar simulator was used to determine PCE and other photovoltaic parameters such as short circut denisty (J_{sc}), open circut voltage (V_{oc}) and fill factor (FF). High efficiency of SiNWs with the length of 0.9 and 0.35µm can be attributed to the better junction area between Si and PEDOT:PSS and shorter diffusion distance of minority carrires. Table 1.1 shows the PV parameters of Si/PEDOT structures with different lengths.

Table 1.1 : Summary of photovoltaic parameters.

SiNWs lengths (µm)	J_{sc} (mA/cm^2)	V_{oc} (V)	FF (%)	PCE (%)
0.35	24.5	0.53	59	7.7
0.9	26.3	0.53	64.2	9.0
2.2	23.1	0.51	60.8	7.2
4.1	18.7	0.49	50.8	4.2

Ge *et al.*[40] fabricated silisium nanowire/cedmium telluride quantum dots/organic hybrid solar cell on n-Si wafer and investigated PV properties. Si nanowire was fabricated by wet chemical etching method and CdTe quantum dots and PEDOT:PSS organic conjugated polymer spin coated to create p-n junction. Figure 1.13 shows the shematic view and top-view SEM images SiNW/CdTeQD/PEDOT:PSS hybrid solar cells.

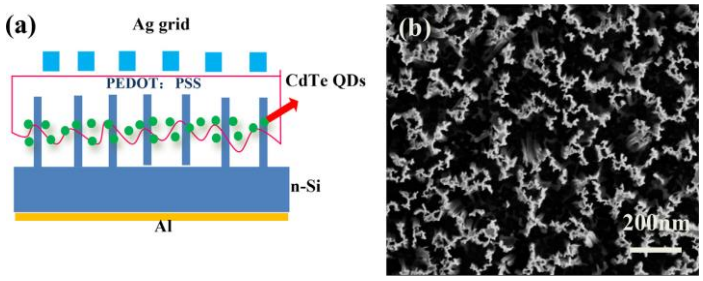

Figure 1.13: (a) Schematic illustration of the SiNW/CdTeQD/PEDOT:PSS hybrid solar cells; (b) SEM image of top-view.

They investigated effect of CdTeQD density by changing cycles of spin coating. 4 samples were prepared, three of them with 4 (sample 1) ,6 (sample 2) and 8 (sample 3) cycles of QDs and one is without quantum dots (sample 0). Table 1.2 summaries of the PV performance of 4 samples.

Table 1.2 : Performance of hybrid solar cell.

	J_{sc} (mA/cm^2)	V_{oc} (V)	FF (%)	PCE (%)
Sample 0	541	29.1	32.5	5.9
Sample 1	501	32.9	42.7	7.0
Sample 2	511	33.5	44.1	7.6
Sample 3	521	30.4	43.2	6.8

QDs can improve absorption of light, however, too many quantum dots may hinder SiNWs to absorb the light.

He *et al.* [41] investigated effect of surface conditions on PV performance. They fabricated Si/PEDOT:PSS solar cell using (100) and (111) Si wafers and compared the performance of hyrdogen terminated (H-Si) and oxide-terminated (SiO_x-Si) surfaces. Table 1.3 summaries the PV parameters of samples.

Table 1.3 : Summary of the PV parameters of hybrid solar cell.

Sample	J_{sc} (mA/cm^2)	V_{oc} (V)	FF (%)	PCE (%)
Si-H (111)	0.28	0.27	19.3	0.02
SiOx-Si (111) d_{ox} 1.5nm	26.4	0.61	65.9	10.6
SiOx-Si (111) d_{ox} 2.1nm	26.3	0.57	34.6	5.2
Si-H (100)	0.46	0.29	16.9	0.02
SiOx-Si (100) d_{ox} 1.8nm	25.8	0.58	62.4	9.4
SiOx-Si (100) d_{ox} 2.3nm	24.7	0.53	25.5	3.4

Thin native SiOx layer is beneficial for charge separation, however, thicker layer would become a barrier for charge transport in solar cell and leading to resistance. Additionally covalent H-Si surface bonding blocks the internal electrical field and prevents the photoexcited holes in Si.

Tsakalakos *et al.* [42] fabricated p-SiNWs using chemical vapor deposition (CVD) method and covered it with n-Si (~40nm) using plasma enhanced chemical vapor deposition (PECVD) to create photovoltaic p-n junction. Al and Ta_2N metals were coated as contact layers by sputtering system. The peak external quntum efficiency (EQE) was measured 12% at 690nm. Figure 1.14 shows the schematic illustration and top view and cross-sectional SEM images of SiNW/CdTeQD/PEDOT:PSS hybrid solar cells.

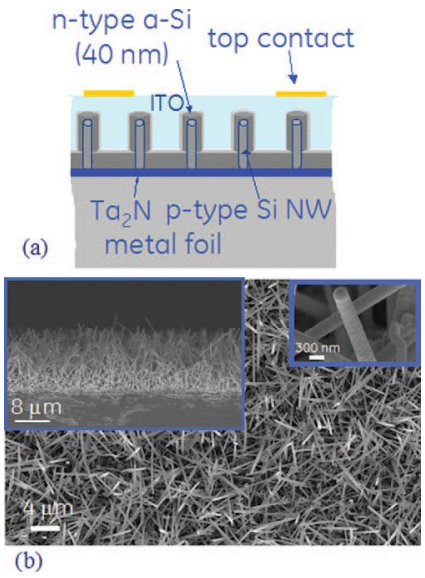

Figure 1.14 : (a) Schematic illustration of the SiNW/CdTeQD/PEDOT:PSS hybrid solar cells; (b) SEM image

Brus *et al.* [43] fabricated hybrid organic-inorganic heterojunction solar cell using P3HT as electron donor and n-Si onto oxide passivated Si (100) surface within the temperature ranging from 283 to 333K. Photovoltaic parameters: J_{sc}=16.25 mA/cm^2, V_{oc}=0.456V, FF=0.45, PCE=3.32% under 100mW/cm^2 AM 1.5 illumination.

Combining carbon nanotubes (CNT) with silicon is another method for increasing solar cell efficiency. Shi *et al.* [44] fabricated CNT-Si junction solar cell with the efficiency 15% by coating TiO_2 antireflection layer and doping CNT with oxidative chemicals. Device fabricated by transferring a semi-transparent CNT film onto n type single crystal Si wafer. By appliying series of doping methods and electronic

gating, power conversion increased from 1.3% to 13.8%. Also TiO_2 colloidal antireflection layer on the top reduced the reflection on surface less than 10% and increased to short-circuit density by 30%. Figure 1.15 shows the illustration and SEM images of Si-CNT-TiO_2 structure.

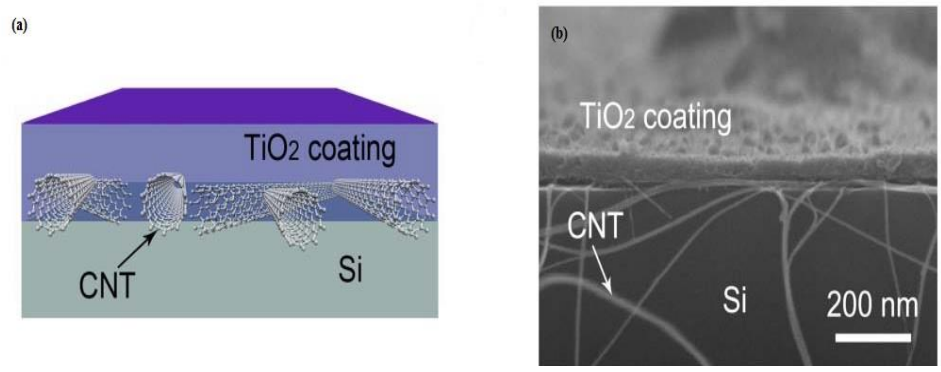

Figure 1.15 : (a) Illustration of Si-CNT-TiO_2 solar cell. (b) Cross-sectional SEM image of the device.

Jia *et al.*[45] achieved high efficiency by doping acid to the silicon-carbon nanotube heterojunction solar cell. Acid infiltration of nanotube significantly increased the cell efficiency by reducing internal resistance. Figure 1.16 shows the illustration and J-V characteriscts of solar cell with and without acid filtration.

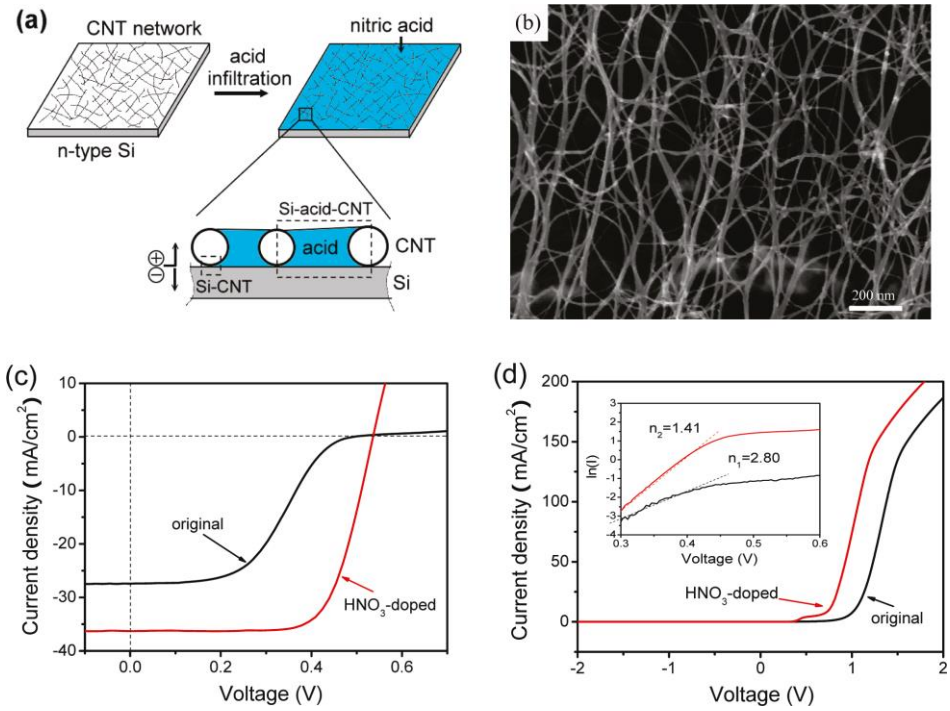

Figure 1.16 : (a) Illustration of the solar cell structure. (b) SEM image of CNT film. (c) J-V characteristics of solar cell before (black) and after (red) acid filtration. (d) Dark J-V cuves of same device before (black) and after (red) acid filtration.

Wang *et al.* [46] fabricated boron doped nanocrystalline silicon/amorphous hybrid solar cell by radio frequency plasma enhanced chemical vapor deposition (RF-PECVD) to improve performance of silicon heterojunction solar cells. P-type Si thin films were fabricated by PECVD system in 180^o with gaseous mixture of SiH_4, Trimethylboron (TMB), and H_2. 3 samples were prepared with different amount of TMB and their PV properties investigated. Table 1.4 shows the fabrication parameters and PV performance of devices.

Table 1.4 : Fabrication parameters and PV performance.

Sample	T_{dep} (^{o}C)	TMB (%)	Band gap (eV)	PCE (%)
1#	180	0.50 (20nm)	1.93	12.16
2#	180	0.75 (20nm)	2.19	15.97
3#	180	0.50 (5nm) 0.75 (15nm)	2.07	17.8

Karaagac *et al.* [47] synthesized ZnO nanowires using hydrothermal technique on both glass and silicon substrate, AGIS polymer film was coated to create p-n junction. ZnO seed layer thicknesses were varied to determine effect of seed layer thickness on PV paramters. Since the seed layer thickness affects NWs homogenity and vertical formation, it changes the solar cell efficiency. In and ITO contact layers were coated by thermal evaporation and DC sputtering, respectively. It was found that quality of ZnO NWs increases in terms of uniformity and oriantation as the thickness of seed layers incereased. Figure 1.17 shows the structure of nanowires.

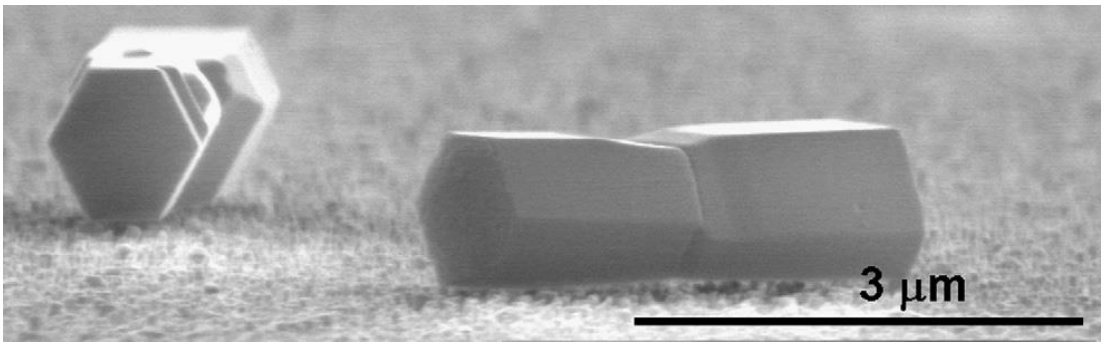

Figure 1.17 : Hexagonal structures of ZnO nanowires.

Also n-SiNWs were fabrcated using electroless etching method onto n-Si wafer and coated by AGIS polymer. In this system PCE was calculated 5.50%.

Tatar *et al.* [48] deposited slanted nanocolumnar a-Si structures by e-beam physical vapor deposition (EB-PVD). Slanted nanocolumnar Si structures were deposited at

the oblique angle α=80° onto n type and p type Si wafer to create heterojunction. Figure 1.18 shows the surface morphology and sontact angle of surfaces.

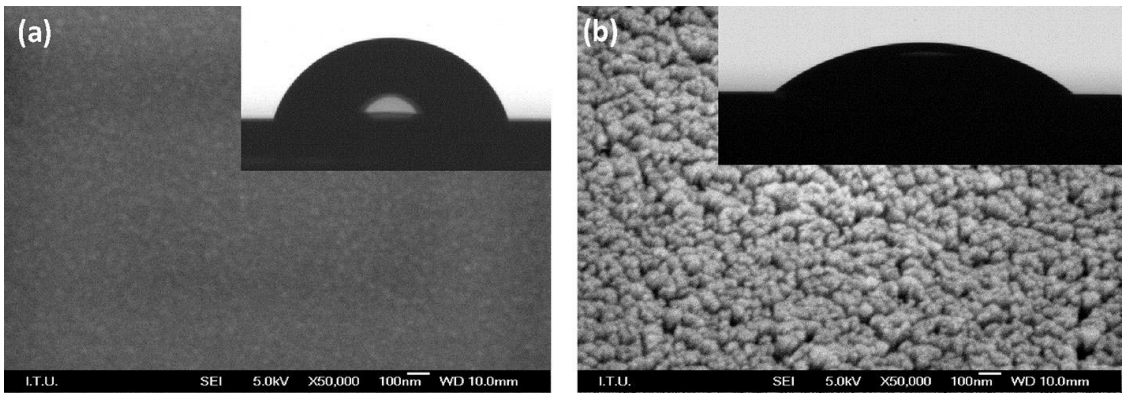

Figure 1.18 : Contact angle and surface morphology of (a) flat a-Si (b) slanted a-Si thin films.

Under 100mW/cm^2 illumination it was found that porous structure of slanted a-Si directly affects PV properties. *Voc* was calculated as 900mV for slanted structure while calculated 410mV for flat surface. Also J_{sc} was obtained 83mA/cm^2 for slanted structure and 41.9mA/cm^2 for flat surface.

2. THEORY

2.1 Properties of Solar Radiation

Solar radiation is a thermal energy emitted by the Sun as a result of fusion process. This process produces temperature of around 15 million degress of Celsius and this energy is released into space in radiation form. The Sun continuously radiates an amount of 3.845×10^{26} W power in all directions of the Earth with small fructions. In order to calculate solar constant value, we assume that there is a sphere around the Sun that has a radius r_{SE}

$$Es = \frac{Radiation\ power}{Area\ of\ \ sphere} = \frac{Psun}{4 \cdot \pi \cdot r_{SE}{}^2} = \frac{3.845 \cdot 10^{26} W}{4 \cdot \pi (1.469 \cdot 10^{11} m)^2} = 1367 W/m^2 \tag{2.1}$$

1367 W/m^2 is called solar constant which denotes irradiance outside the Earth's atmosphere. The spectrum outside the Earth's atmosphere called AM 0 refers to Air mass 0. As can be seen at figure 2.1 spectrum changes when sunlight passes through the atmosphere due to the reflection, absorption, rayleight scattering and dust particles.

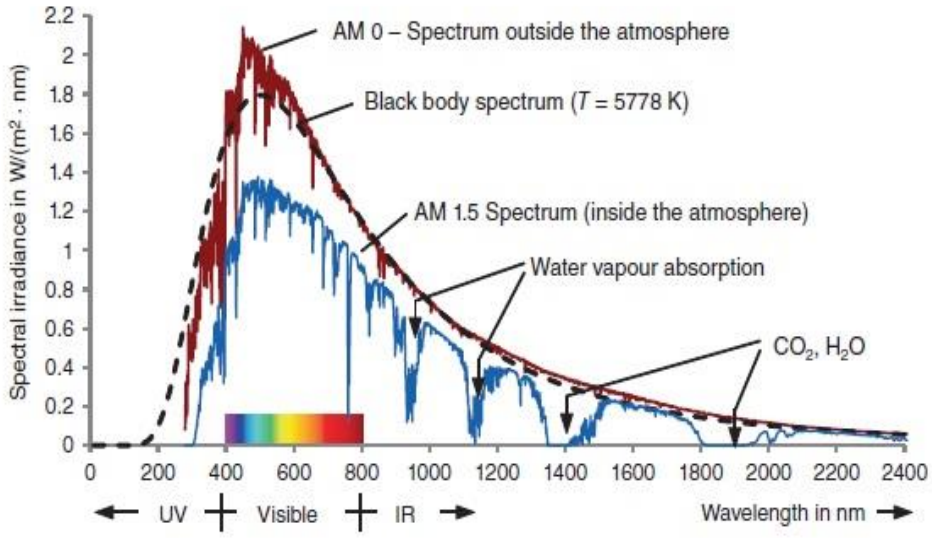

Figure 2.1 : Spectrum outside and inside atmosphere [5].

2.2 Fundementals of Semiconductor Physics

2.2.1 Bohr's atomic model

In 1911 Bohr propesed his quantized shell model of atom to explain how electrons have stable orbit around nucleus. The Rutherford model was unstable because according to classical mechanics and electromagnetic theory, any charged particle decelerating emits electromagnetic radiation thus electron would lose energy and spiral into nucleus. Bohr modified the Rutherford model. According to his first postulate there are only certain discrete shells permitted for an electron. Each of these shell stands for a particular path radius that reperesent the respective energy state of an electron. Radiation only occurs when one electron jumps from one shell to another. According to the Bohr's second postulate the transfer of an electron from one shell to another occurs under the emission or absorption of electromagnetic radiation. The shells are designated with the letter of K, L, M and so on. Figure 2.2 shows the possible energy states for hydrogen atom.

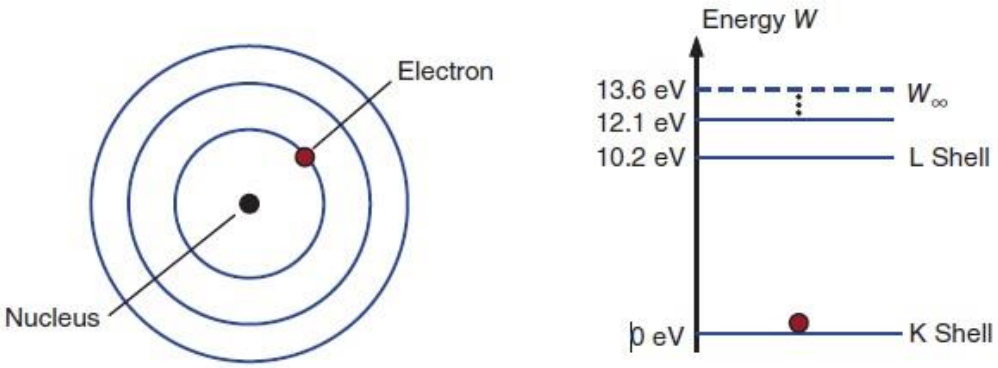

Figure 2.2 : Structure and energy model of hydrogen atom [5].

In the basic state electron is stuated in K shell. If the electron is moved to the L shell than energy of 10.2eV is necessary in order to seperate electron. This energy is called as ionizing energy W_∞. Figure 2.3 shows the emission and absorption of the light. The frequency of this radiation is determined by the following equation.

$$\Delta W = |W_2 - W_1| = h \cdot \nu = \frac{h \cdot c}{\lambda} \tag{2.2}$$

W_1: energy before transfer

W_2: energy after transfer

h: Planck's constant = $6.6 \cdot 10^{-34}$ Ws^{-1}

ν: frequency

c: speed of light in a vacuum = $3 \cdot 10^{8}$ m/s

λ: wavelength

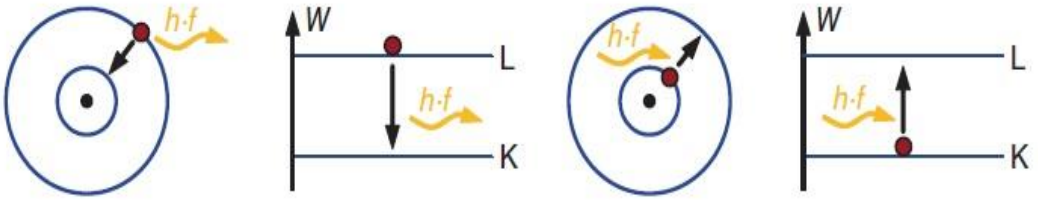

Figure 2.3 : Schematic depiction of the emission and absorption of light [5].

2.2.2 Band model of semiconductors

We know that there are defined, dicrete energy levels for electrons in an individual atom. What if we bring two atoms close together? There occurs mutual coupling of atoms. The energy conditions change and each state divides into two individual states. In the case of three coupled atoms then three new levels occur. If infinite number of electrons can be coupled together then individual levels will hardly be recognized. In this case we can talk about energy bands. The energy bands show all energy levels that are permitted for an electron. Figure 2.4 shows the coupling of atoms and formation of energy bands.

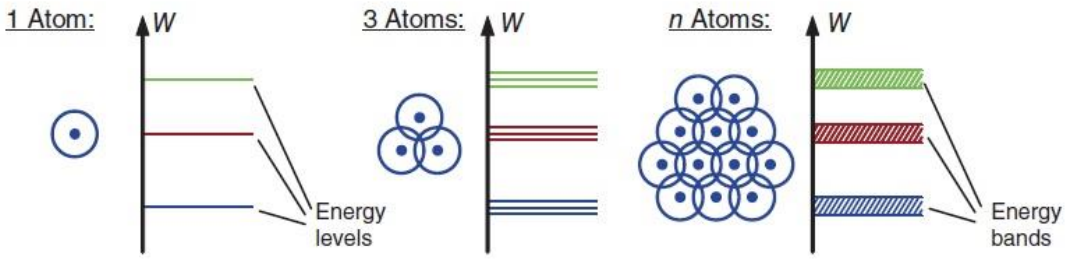

Figure 2.4 : Origin of the energy bands in a semiconductor crystal: the coupling of the atom leads to a spreading of the energy level. For n→∞ in this results in continuous energy bands [5].

The highest band still occupied by electrons is decisive for the electrical relationship for solid-state body. As this is occupied by the valence electron it is called the valence band. The first unoccupied is called conduction band. In order to enter into

conduction band, an electron must first overcome the forbidden zone which called band gap (ΔW_G). The width of bandgap decides the amount of energy that an electron needs to move into the conduction band.

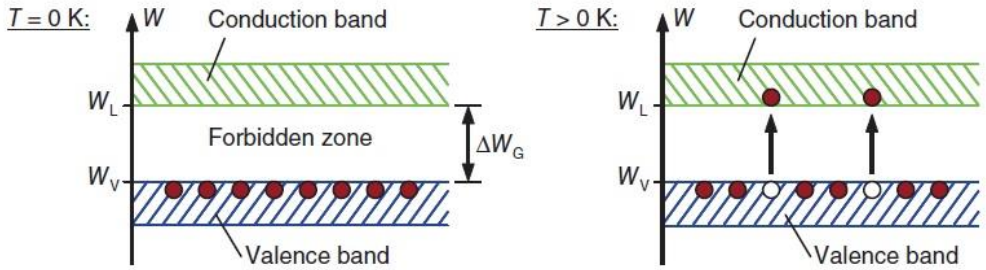

Figure 2.5 : Valence and conduction band for silicon: With rising temepratures individual electrons rise into conduction band [5].

At absolute zero temperature (T=0K) the valence electron remain fixed in their bonds so the crystal is unable to conduct electrical current as no free charge carriers are available. If the temeperature is increased then electrons start to move into conduction banddue to heat oscillations. Figure 2.5 shows the how temperature affects individual electrons.

In the case of insulators the band gap is very big. Insulators are typically materials whose bandgap is greater than about 3 eV. This means almost no free electrons are available at high temepratures. At low temperature semiconductros act as insulators. At medium temperatures, however, the conductivity begins to increase until very high temperatures (over 200ºC). The higher the temperature, the higher the conductivity. Metals have special case. Their valence and conduction band overlap so they possess high degree of conducitivity even at low temperetures. Figure 2.6 shows the schematic description of energy bands of insulator, semiconductor and metals.

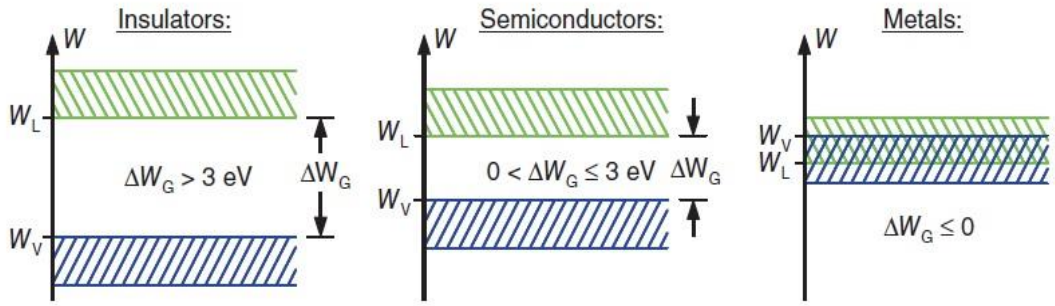

Figure 2.6 : Schematic description of energy bands of insulators, semiconductors and metals [5].

2.2.3 Doping of semiconductors

Semiconductors have another important property alongside the temperature: their conductivity critically depends on the type and concentration of impurities. According to the position of energy levels of the atom in the bandgap, there two major types of impurities.

The energy level of donor atoms is below the bottom of conduction band. The impurity atom can easily be ionized to contribute an electron to the conduction band. For silicon and germanium, atoms from group V of the periodic table (N, P, As and Sb) are effective donors. The Fermi distribution is valid and but the Fermi level is shifted towards the conduction band as shown in Figure 2.7. The concentration of free electrons in a n-type semiconductor, approximately equals to the concentration of donor atoms.

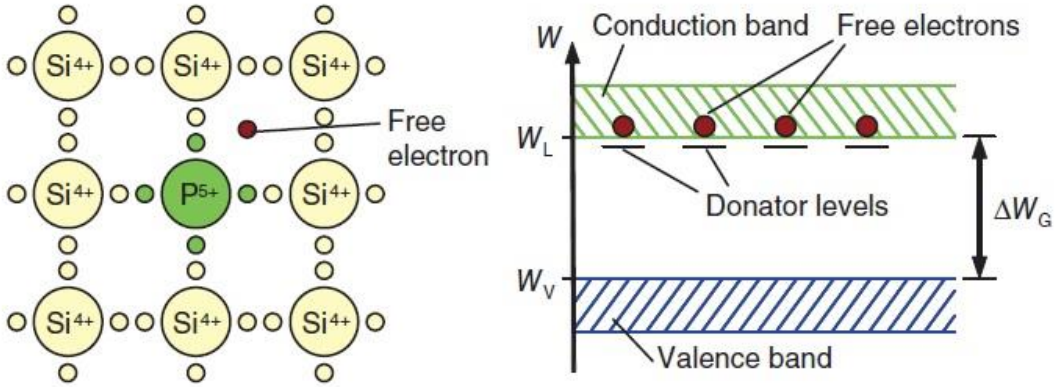

Figure 2.7 : n doping of semiconductor; one of the five valence electrons of the phosphorous atom is not necessary for the bong therefore available as a free electron. Because of the doping there is a new nergy level in the band diagram just below the conduction band edge [5].

Assume that the concentration of donor atoms is N_D, If the temperature is moderately high, all donor atoms could be ionized. The concentration of free electrons in an n-type semiconductor, n_n, approximately equals the concentration of donor atoms,

$$n_n = N_D \tag{2.3}$$

On the other hand, the energy level of acceptor atoms is above the top of the valence band. An electron in valence band can easily be trapped by the acceptor atoms and leave a hole in valence band. For silicon and germanium, atoms from group IIIA (B, Al, Ga, and In) are effective acceptors. The Fermi distribution is still valid but the

Fermi level is shifted toward the valence band as shown in Figure 2.8. The concentration of holes in p-type semiconductor, approximately equals to the acceptor concentration.

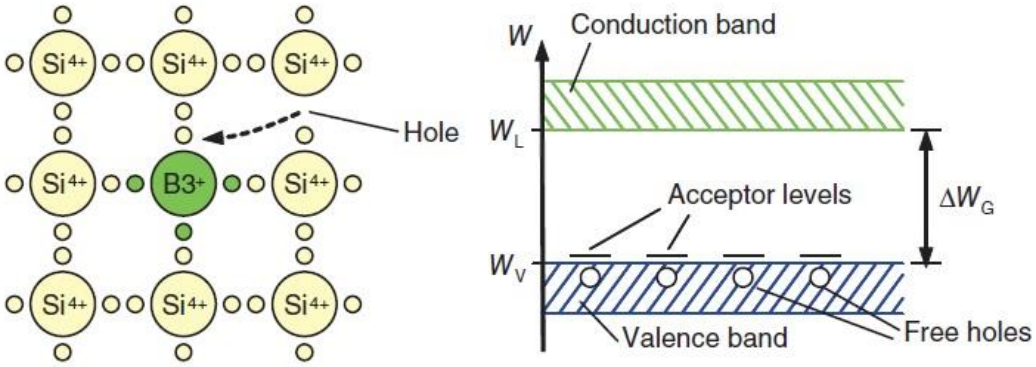

Figure 2.8 : Example of p-doping of a silicon crystal with a boron atom: one of the four links remains opne a the boron atom can only offer three valence electrons. A neighboring electrons moves into this binding and thus "generates" a hole [5].

Assume that concentration of acceptor atoms is N_A. If the temperature is moderately high all acceptor atoms become negative ions. The concentration of holes in a p-type semiconductor, p_p, approximately equals to the acceptor concentration,

$$p_p = N_A \tag{2.4}$$

In both cases, the product of concentration of free electrons and holes equals to the square of the intrinsic career concentration,

$$n_n p_n = p_p n_p = n_i^2 \tag{2.5}$$

p_n: the hole concentration of a n-type semiconductor

n_p: the free-electron concentration of a p-type semiconductor

Each is a minority career concentration.

2.3 Solar Cell Operation

2.3.1 P-n junction

A p-n junction can be conceived as a two doped semiconductor of n-type and p-type that have surface in common. When both semiconductors are separated, they are electrically nautral. When they get in touch, the majority carriers of n-type

semiconductors (electrons) begin to diffuse into p-type and the majority carriers of –type semiconductor (holes) begin to diffuse into n-type semiconductor. Holes coming from p-type recombine with electrons in n-type semiconductor. Inside the n-type region near the the junction, where there are no more majority charges, a depletion is observed and the corresponding zone remains with fixed positive charges. In the same way electrons coming from n-type region recombine with holes in p-type semiconductor. Inside the p-type region, near the junction, where there are no more majority charges, a depletion is observed and the corresponding zone remains with fixed negative charges. Figure 2.9 shows the schematic representation of a p-n junction. Eletrons flow from the n-side to p-side and occupy the holes. On the n-side, fixed positive charges remain behind, on the p-side fied negative charges are generated.

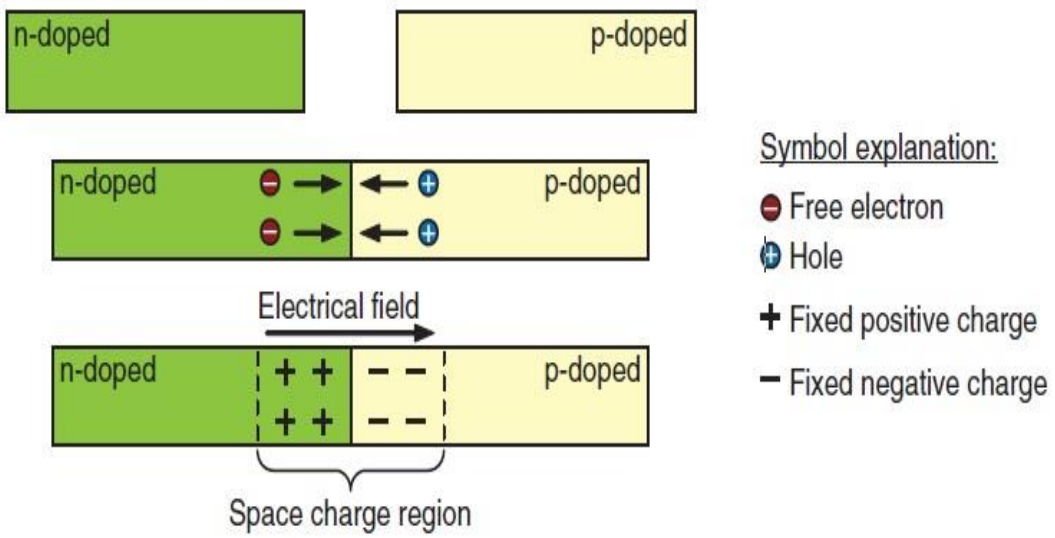

Figure 2.9 : The p-n junction: Electrons flow from the n-side to the p-side and there occupy the holes. On the n-side, fixed positive charges remain behind; on the p-side fixed negative charges are generated [5].

Fermi level is the maximum energy level occupied by an electron at 0K. The Fermi energy of an undoped semiconductor is in the middle of forbidden region. However as soon as the semiconductor is n-doped, number of electrons in conduction band rises and with this so does the Fermi level. The reverse case occurs in p-doping region. Since most of the electrons are situated in valence band the Fermi level is just above the edge of valence band. If the p and n regions are brought together, then the Fermi energy in thermal equilibrium must be at the same level in both region. Figure 2.10 shows the p-n junction by means of the Fermi energies of n and p doped sides.

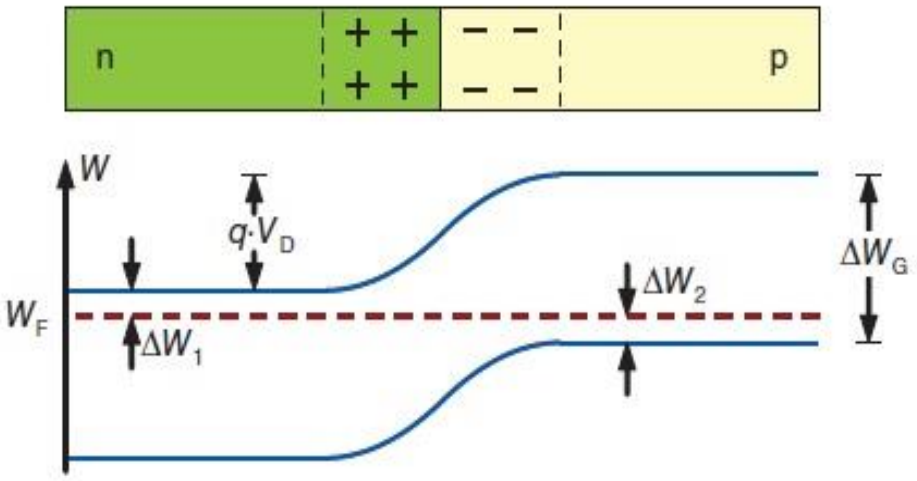

Figure 2.10 : Determination of the diffusion voltage VD of the p-n junction by means of the Fremi energies of n- and p-doped sides [49].

As a result p-type side of space charge region is negativly charged, n-type side of the space charged region is positively charged. This cause an electrical field across the space charge region which is directed from the n-type region to the p-type region. The electrical field forces the the electrons in p-type semiconductor to move back to the n-type semiconductor. Similarly the electrical field forces the hole in n-type semiconductor to move back to p-type semiconductor. In this case p-n junction is in equilibrium and there is no net current.

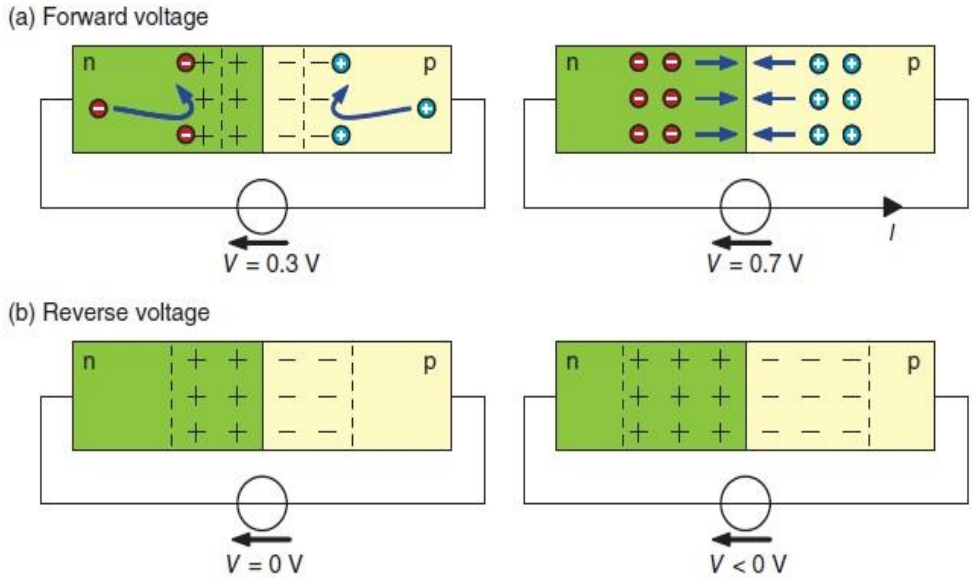

Figure 2.11 : Behavior of the p-n junction with applied voltage: when V rises the space charge region is decued until t finally disappears completely and a current can flow. In the case of reverse voltage the diode blocks and the spece charge region enlarged [5].

If we apply a riverse bias voltage in such system in dark then the depletion zone gets wider, the diffusion of majority charge carriers surpressed and only a small current is genereted. If we apply a forward bias voltage in such system in dark then the depletion zone gets smaller The diffusion of majority charge carriers is significantly enhaced, the p-n junction becomes conductive and it is able to generate a current. Figure 2.11 shows the behavior of the p-n junction with applied voltage: when V rises the space charge region is decued until t finally disappears completely and a current can flow. In the case of reverse voltage the diode blocks and the spece charge region enlarged.

2.3.2 Interaction with light

Incident light photons lift individual electrons from valence band into the conduction band. In order to trigger this effect, the energy of photons W_{ph} must be higher than bandgap.

$$W_{ph} = h \cdot v = \Delta W_G \tag{2.6}$$

Figure 2.12 shows the incident light ray in a semiconductor crystal. The photon is absorbed only with sufficient light energy and electron is raised into the conduction band 5.

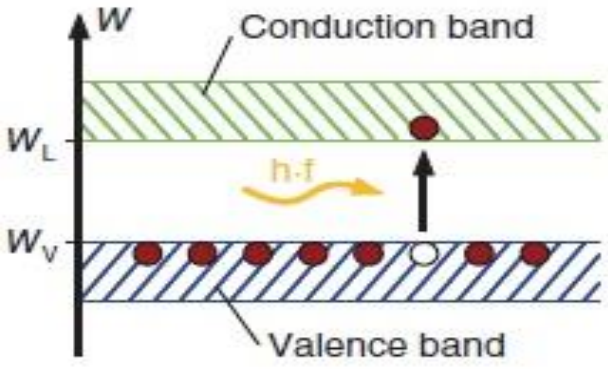

Figure 2.12 : Principle of light absorption in the semiconductor. The photon is absorbed only with sufficient light energy and electron is raised into the conduction band [5].

In dark p-n junction behaves like a diode which is a electrical element that if you applied a forward bias valtage on it, then it becomes conductor in one direction. However if you apply reverse voltage it blocks the current. Their main function is to allow electrical current in one direction and block in the opposite direction. The relation between current and voltage of p-n junction in dark illustrated in figure 2.13.

Figure 2.13: Symbol and I/V characteristic curve of a p-n diode: in the forward direction diode there are high currents, in the reverse direction diode only conducts from threshold voltage [5].

As soon as light shines on the diode a current that is independent on the voltage V is added to the diode characteristic curve. Free electrons and holes generated by light absorption are separated from the field of space charge region. Figure 2.14 shows the p-n junction under illumination and current-voltage characteristic of p-n diode in dark and illumination conditions.

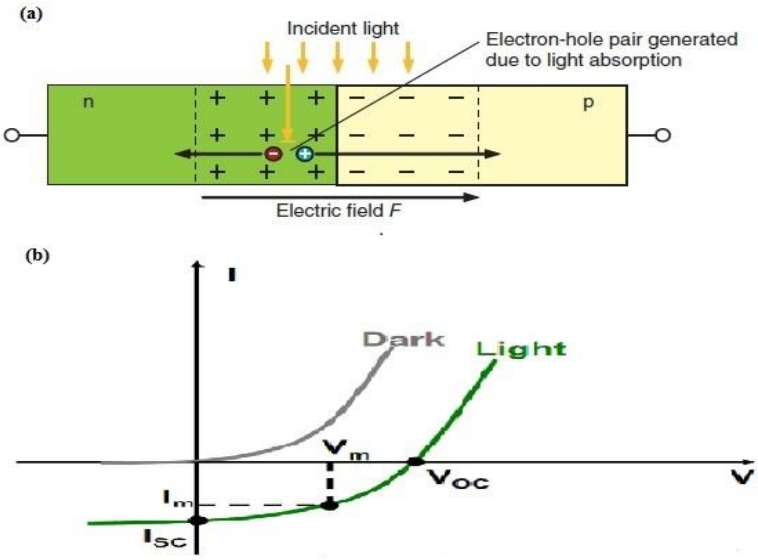

Figure 2.14 : (a) lighted p-n junction: electron and holes genreted bu light absorption are separated from the field of the space charge region and "brough home" (b) I/V curve of p-n diode under dark and illumination conditions [5].

2.3.3 Characterization and efficiency

It will be noticed that the curve produced under illumination is simply shifted from the other curve by a value of I_{sc}, which represents the constant generation of current by light. This value is called short-circut current, because it is a current generated under the light at zero voltage. The value of V_{oc}, in contrary, open-circuit voltage, voltage under illumination at zero current.

The operating point, at which the maximum power is provided is called the Maximum Power Point (MPP). As the power of a working point always corresponds to the surface of I·V, this area must be maxium in the case of MPP.

The fill factor (FF) describes the relationship of MPP and the product from open-circuit voltage and short-circuit current. As can be seen at figure 2.15, FF shows the size of the area under the MPP working, compared to the area $V_{oc} \cdot I_{sc}$.

$$FF = \frac{V_{MPP} \cdot I_{MPP}}{V_{OC} \cdot I_{SC}} = \frac{P_{MPP}}{V_{oc} \cdot I_{SC}} \tag{2.7}$$

The fill factor is a measure for the quality of a cell; typical values for silicon solar cells are between 0.75-0.85.

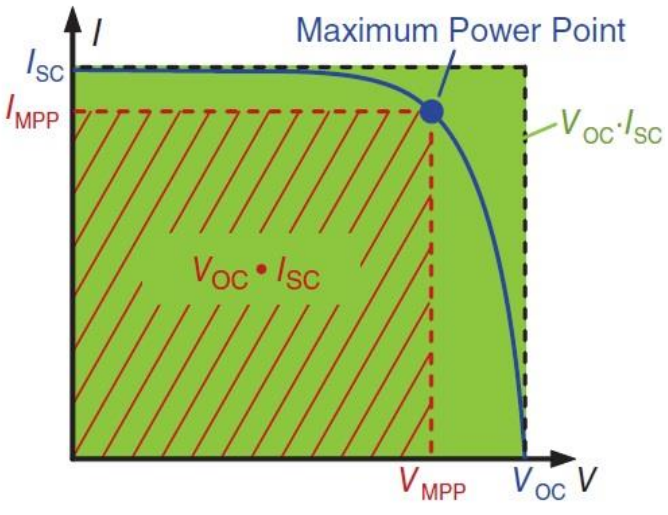

Figure 2.15 : The fill factor gives the relationship of the shaded red to the green background surface [5].

The efficiency of a solar cell is defined as the ratio between the maximum power produced and the power of solar radiation striking the PV module. The efficiency is defined as follows:

$$\eta = \frac{P_{MPP}}{E \cdot S} \tag{2.8}$$

η: Power conversion efficiency of a solar cell

E: illumination (W/m^2)

S: surface of the module

3. MATERIALS AND METHODS

3.1 Silicon Wafer

Silicon wafer also known as substarate is a thin slice of semiconductor material used in electronics, integrated circuts, photovoltaics for solar cells [50]. Silicon wafers are available in different diameters from 1inch (25.4mm) to 11.8inches (300mm) [51]. Silicon wafers can be both p and n type and have <100> or <111> crystal oritentations [52]. Figure 3.1 shows the silicon wafer in different diameters.

Figure 3.1 : Silicon wafers in different diameters [53].

3.2 Aluminum and Silver

Aluminum (Al) was used as thin film back contact and silver (Ag) was used as front grid contact. Aluminum is the most abundant metal and the third most abundant element in the Earth. It is nonmagnetic, soft, ductile metal. Atomic number is 13. Silver is a transition metal with high electrical and thermal conductivity. Atomc number is 47 [54]. Figure 3.2 shows the aluminum crucible materials.

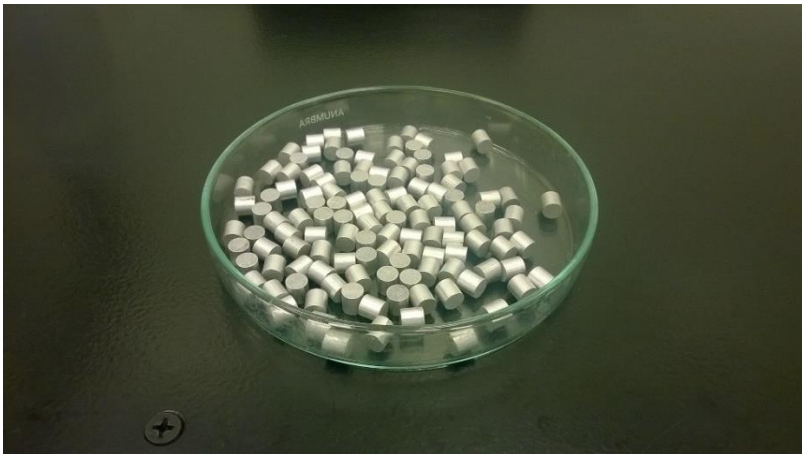

Figure 3.2 : Aluminum crucible materials.

3.3 Silicon

Silicon is extremely important for photovoltaic devices. It has the atomic number 14 and situated in the fourth main group. The K and L shells are full, there are four electrons in the top shell which means it possesses four valence electrons. Silicon is the eighth most common element in the Earth by mass, however very rarely found as pure. Figure 3.3 shows the structure of a silicon.

Silicon is solid at room temperature. It has relatively high melting and boiling point with 1414 and 3265^{o}C, respectively. In crystalline form, pure silicon has a gray color and metallic luster [55].

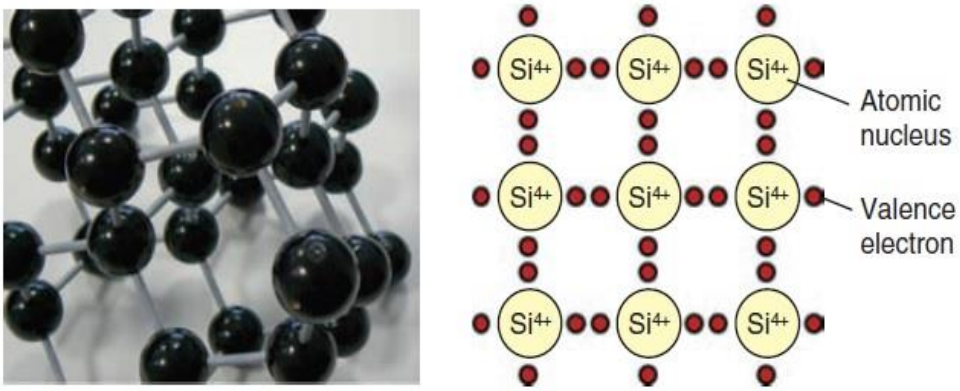

Figure 3.3: Structure of a silicon crystal: The left figure shows the spherical model and the right the two-dimensional depiction [5].

Amorphous silicon is the non-crystalline form of silicon. It has extremely irregular structure of silicon atoms. Amarphous silicon consists of multitude open bonds that are called dangling bonds. Amarphous silicon differs from other variations, such as

monocrystalline and polycrystalline silicon, has small grains known as crystallites. Figure shows the picture of amorphous silicon crucible materials.

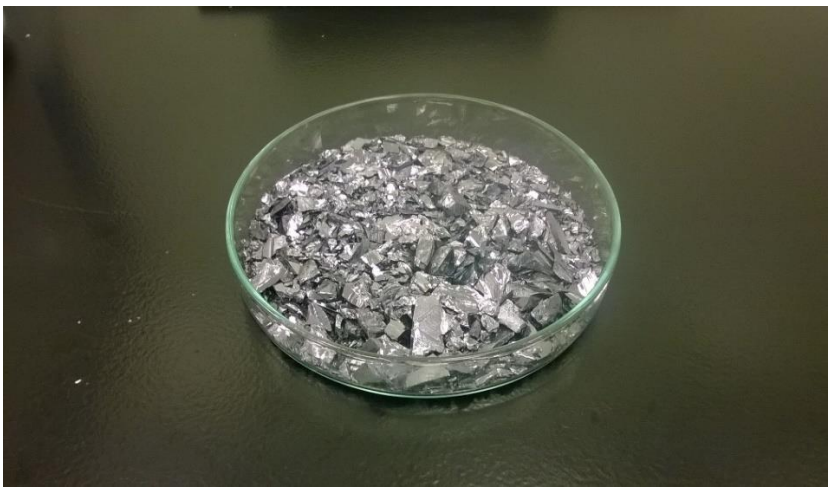

Figure 3.4: Amorphous silicon crucible materials.

Monocrystalline silicon consist of silicon in which the crystal lattice of entire solid is continuous and unbroken to its edges. Mono-Si cells have the highest efficiency in commercial market with 25.6% while poly crystalline cells have 20.8% efficiency [56].

Polycrystalline silicon are composed of a number of smaller crystals. Polycrystalline silicon materils differ from amaorphous and poly-Si consist of multiple small silicon crystals. These crystals are giving the material flake effect. Figure 3.5 shows the atomic structure of mono-Si, poly-Si and amorphous silicon.

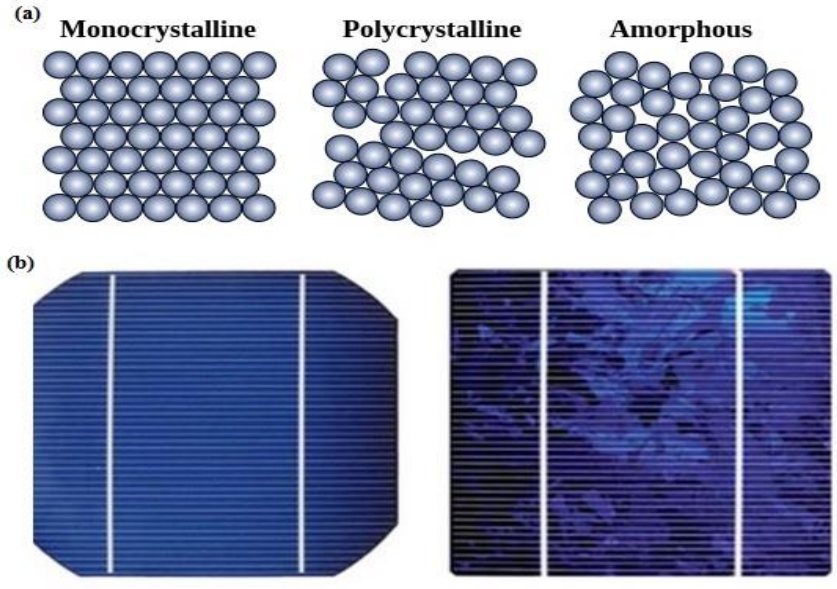

Figure 3.5: (a) shows the atomic structure of mono-Si, poly-Si and amorphous silicon [57] (b) mono crystalline (left) and poly crystalline (right) silicon solar cells [58].

3.4 PEDOT:PSS

Poly(3,4-ethylenedioxythiopehene):poly(styrenesulfonate) (PEDOT:PSS) is a transparent, hole-conducting polymer with adjustable electrical parameters. Its work function in the range of between 4.8 and 5.2eV and conductivity up to 1000S/cm. PEDOT:PSS can easily be deposited by spin, spray and dip coating which are suitable for the deposition of any aqueous solution at the temperature of 100°C under atmospheric pressure conditions [59]. On the n-type silicon, PEDOT:PSS forms and organic-silicon junction with remarkably high saturation and power conversion efficiency (PCE) [60]. Figure 3.6 shows the structure of PEDOT:PSS.

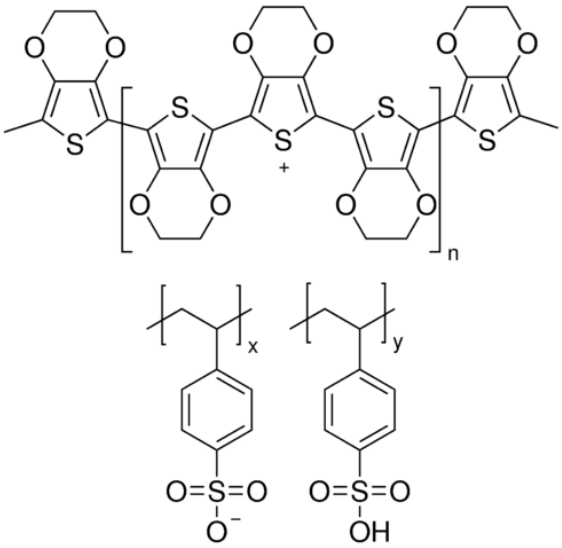

Figure 3.6 : PEDOT:PSS [61].

3.5 Physical Vapor Deposition (PVD)

PVD process is basically coating a substrate by vaporizing or sputtering material in a vacuum environment. A wide range of metal, chemical compounds and composition can be deposited on a surface. This process exhibits fine grain size, dense structure and can be carried out relatively lower temperatures compared to other methods such as chemical vapor deposition (CVD). PVD process works in the range of 150-550°C which makes possible to choose great variety of substrate. Almost all kinds of tool steel can be used.

There are three major types PVD process. In thermal evaporation coating material directly heated up, vaporized and deposited on a desirable surface inside vacuum chamber. For materials possess higher evaporation temperature electron beam

evaporation is preferred. In this type of evaporation electron beam generated by an electron gun or incandescent flament cathode. Emitted electrons are accelerated towards crucible holding the evaporation material by electrical field. Also a magnetic field is applied to move the e-beam and scan the surface of evaporation material. When e-beam falls down the material's surface, material heats up and starts to evaporate. This mechanism provides several advantages over the similar processes. First, adjusting accelerating voltage and changing magnetic field, the electron beam can be localized, unfocused, accelerated or retarded. This ability allows us to control deposition rate in a wide range from nanometer per minute to micron. Also evaporation materials are deposited with limiteless shape and forms with high purity including materials with high melting point such as W, Ta, C, etc. E-beam evaporation also offers us excellent material utilization, precise film composition, uniform deposition and minimum contamination [62]. Figure 3.7 shows the illustration of e-beam evaporation system.

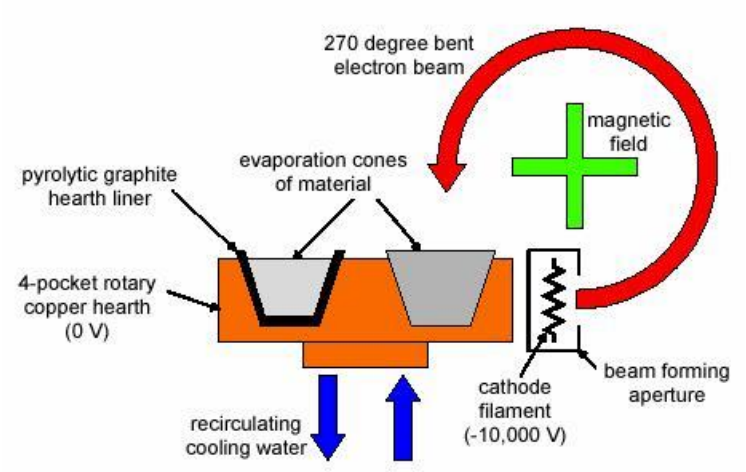

Figure 3.7 : Illustration of e-beam evaporation system [63].

The PVD deposition techniques discussed so far basically based on thermal. However sputtering is a different technique which allows us deposition material under its evaporation temperature. In this process highly energetic ions are bombared to the material surface creating a plasma using an inert gas mostly Argon. Properties of thin film depending on ion energy range (1 eV to 10.000 keV). The interaction of energetic ions with surfaces will also created a variety of interaction besides sputtering, such as secondary atoms, neutrals, photons, X-rays. These interactions play an important role during film deposition. For example emission of secondary

electrons is essential for maintaining discharged plasma [62]. Figure 3.8 shows the sputtering process and film formation.

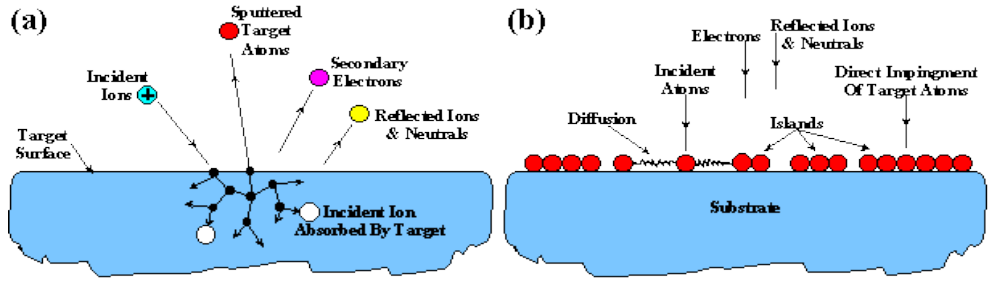

Figure 3.8 : (a) Illustrating diagram of sputtering process at the target, (b) film formation on substrate [64].

3.6 Glancing Angle Deposition (GLAD) and Structured Thin Films (STF)

Glancing angle deposition (GLAD) provides oblique deposition and substrate motion to engineer thin film microstructures in three dimension on nano scale. Using this technique, we can obtain "zigzag", "staircase", "chiral", "helical" and various type of nanostructures from various metals with controllable morphologies [65]. Figure 3.9 shows the increasing control of GLAD technique in past 15 years and Figure 3.10 shows the schematic of GLAD process.

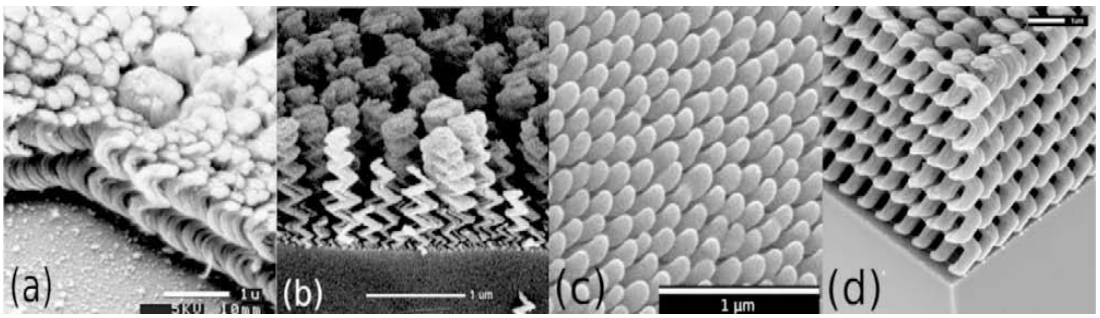

Figure 3.9 : SEM images are showing increasing control of offered by the GLAD technique over the past 15 years: (a)erly spirals, (b) early chevrons, (c) top-down view of Alq3 spirals, and (d) Si square spiral. (a) and (b) are from 1994, (c) and (d) are from 2007. All scale bars are 1µm [66].

These types of nanostructures are called as structured thin films (STF). These structures have wide range of applications such as optical filters [67], photonic crystals, gas sensors [68], magnetic storage [69], microchannels [70], biosensors [71], anti-reflection coatings [72], catalysts depending on their material, size and gometrical shape.

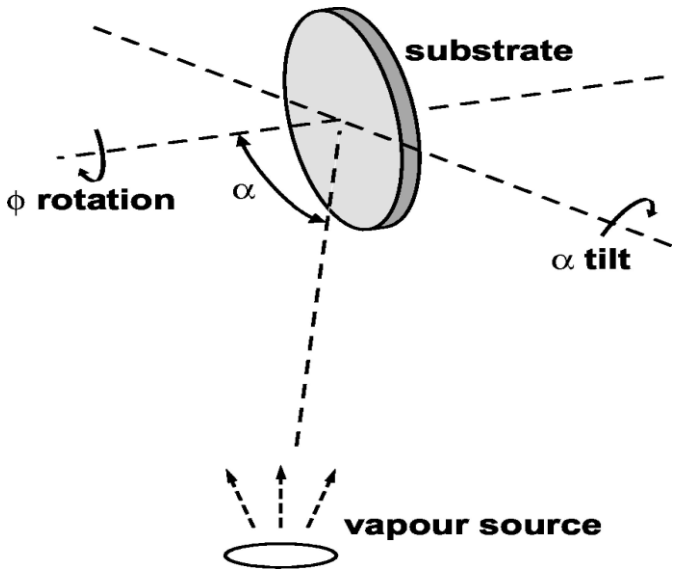

Figure 3.10 : Schematic of GLAD process. Φ is substrate rotation and α is vapor incident angle [73].

The column inclination angle (β), is the angle between film normal and vapor incident angle (α). It depends on many factors such as film temperature, deposition flux, gas pressure, gas compostion and flux energetics [73]. Figure 3.11 shows the schematic of depostion flux and film orientation with the angle definitions. α is the vapor incident angle and β is the columnar microstructure inclinationa angle measured from substarate normal.

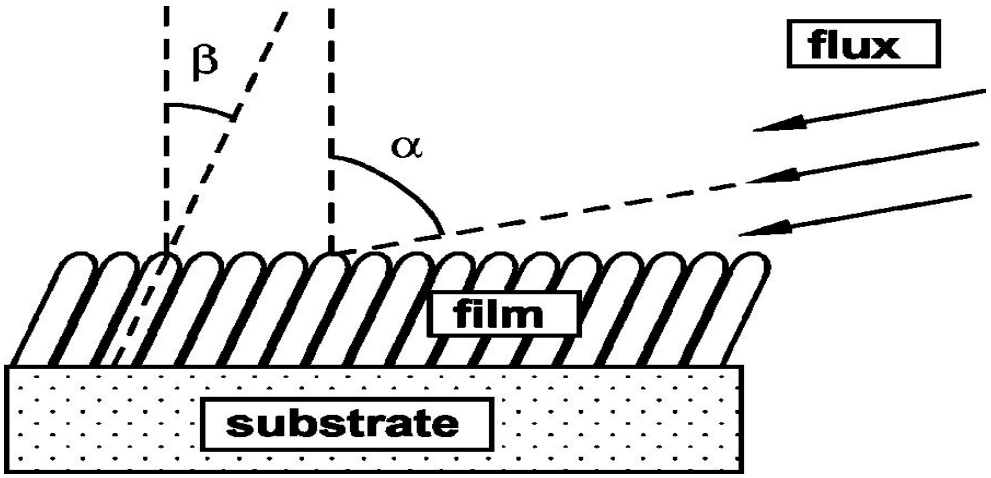

Figure 3.11 : Schematic of deposition flux and film orientation with angle definitions. α is the vapor incident angle and β is the columnar microstrcture inclination angle measured from the substrate normal [73].

However, there is a fix relationship between vapor incident angle and columnar angle based on the geometrical analyses in fixed deposition conditions shown in figure 3.12.

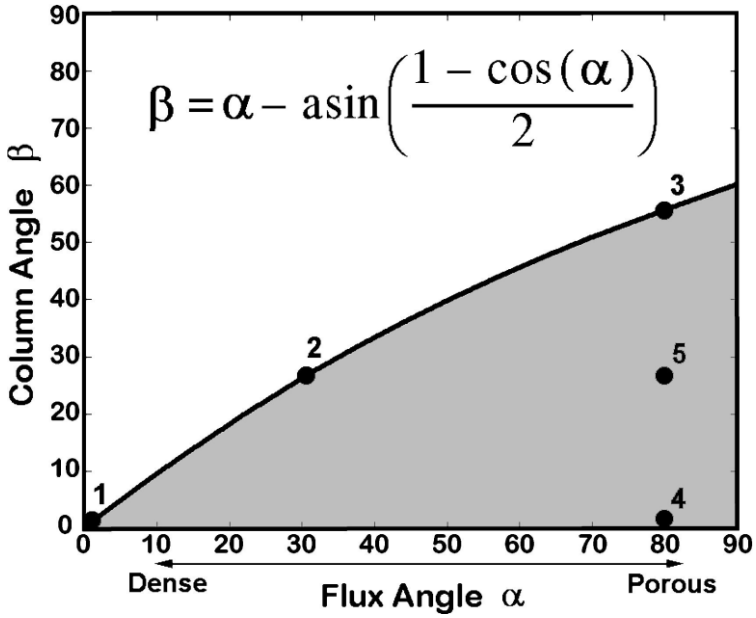

Figure 3.12 : Fixed relationship between incident vapor flux and columnar growth angle for a fixed set of deposition conditions (material, temperature, gas composition, pressure and vapor energetics) [74].

Since the porosity of thin films is depending on incident vapor angle, column growth angle cannot be choosen independently. If large columnar angle (more parallel to substrate) is desired, the flux must be deposited at large oblique angle which is resulting in a very porous film. If dense film is desired flux must arrive more perpendicular to the substrate and resulting dense microstructure [75].

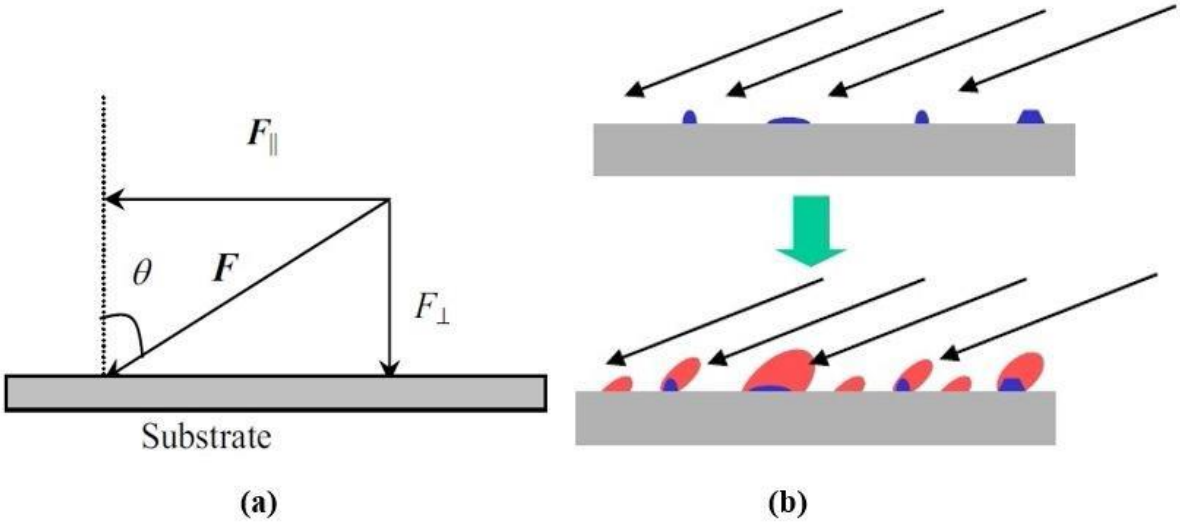

Figure 3.13 : (a) the incident flux can be decomposed into two different components, (b) form of shadowing islands and columnar structures due to shadowing effect [76].

Vapor angle has two dimensions, a vertical component and a lateral component. During the deposition of thin film, first arriving atoms form islands on flat substrate randomly. As deposition proceeds these islands will act as shadowing centers and all tallest islands will receive more impinging atoms compared to shorter areas (shadowing effect). As can be seen at figure 3.13 lateral component of the incident vapor is the source for shadowing effect. This process will continue until tallest islands grow into columns and columnar film will be formed.

3.7 Spin Coater

Spin coating is a procedure used to deposit uniform film to flat substrates. Small amount of coating material is droped on the center of substrate then rotated in high speed (typically around 300rpm). Film thickness and other properties will depend on the nature of fluidic materials such as viscosity, drying rate, percent solids, surface tension etc [77]. Figure 3.14 shows the schematic of application of spin coating method.

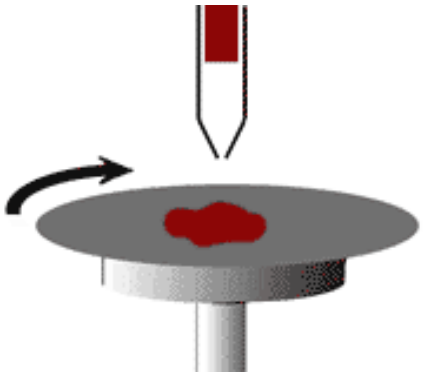

Figure 3.14 : Application of spin coating [77].

4. EXPERIMENTS AND RESULTS

4.1 Fabrication

First 250nm aluminum contact layer were deposited onto p-type (100) silicon wafer. Then highly doped (10^{18} atoms/cm^{-3}) n-type silicon structured thin films and flat surface deposited onto aluminum surface by e-beam deposition technique using Kurt J. Lesker equipment. Silicon films' thicknesses were about 400nm for all samples. Structured thin films were deposited at 80^{o} to form slanted structures with no rotation and at 80^{o} with 25rpm to form vertical columnar structures. Highly conductive and transperant PEDOT:PSS (Heraeus-Clevios) was coated onto silicon structured thin films and flat surface. First PEDOT:PSS was droped onto surface and left for 1min. then it was spin coated with 2000rpm/min twice. Finally silver metal grid top electrodes deposited onto PEDOT:PSS surface by thermal evaporation. Complete cell sizes are about 1cm x 1cm. Figure 4.1 shows the schematic presentation of fabrcation process and device structure.

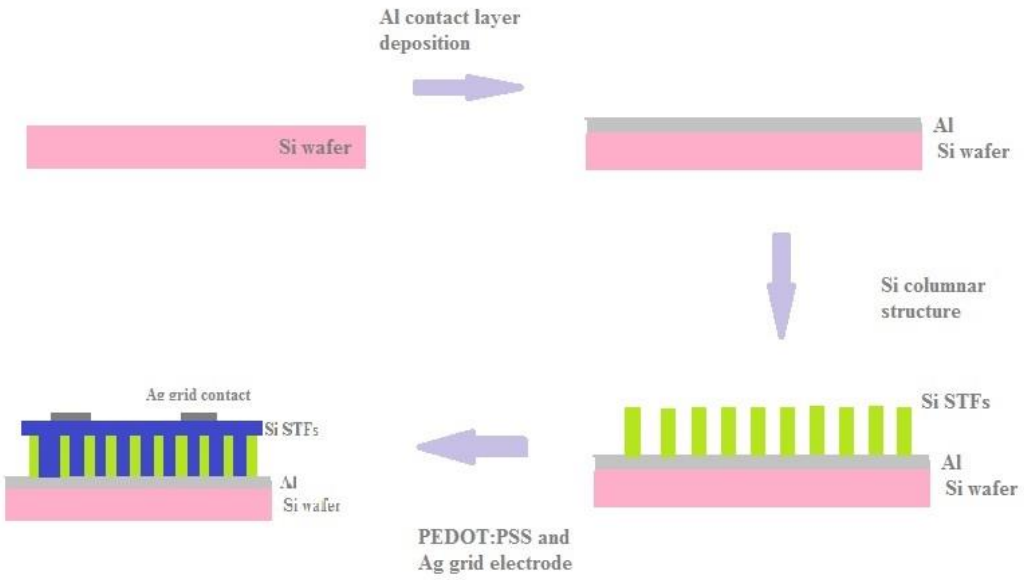

Figure 4.1 : Fabrication process of Si/PEDOT structure.

4.2 Imaging and Charaterization

Figure 4.2 shows the cross-sectional SEM images of columnar structures and flat surfaces. PEDOT:PSS can be seen at between columnar structures and top of the flat surface. As can be seen at (a) and (b) PEDOT has better distrubution on columnar structures compared to flat surfaces. This increases p-n junction area.

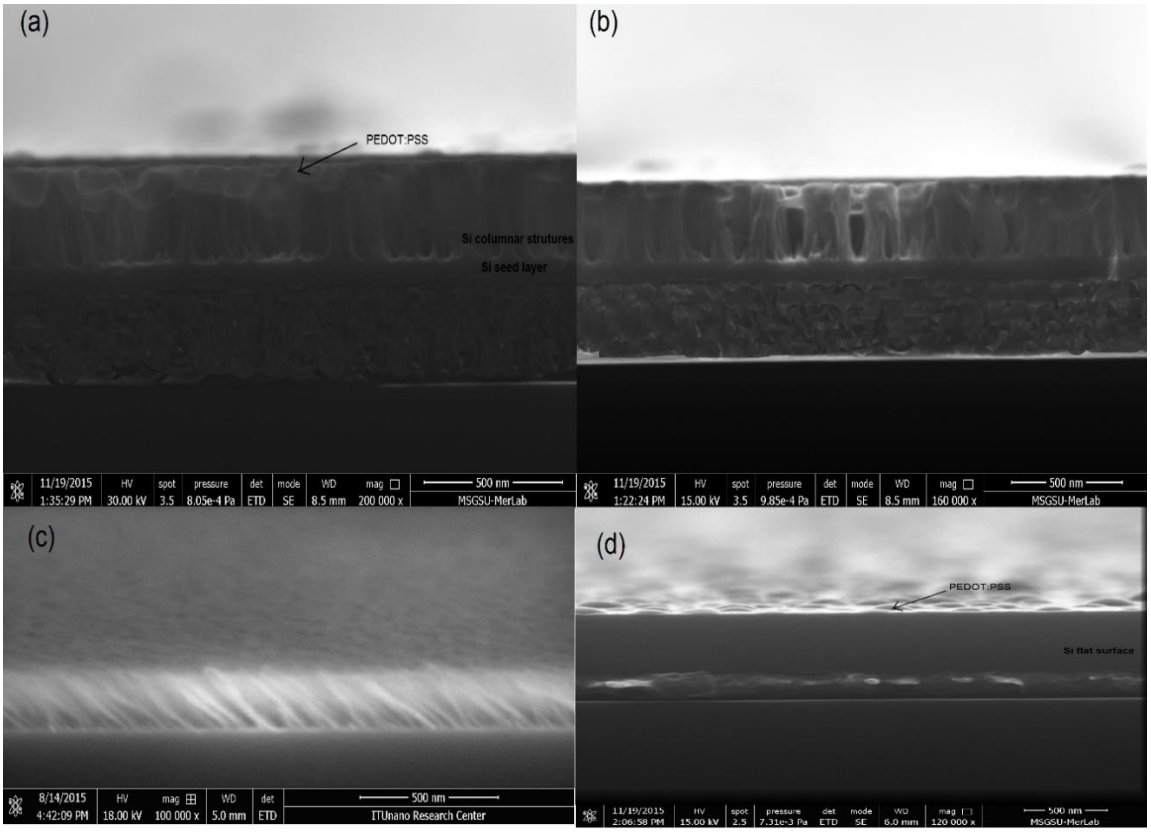

Figure 4.2 : Cross-sectional sem images of silicon thin films with PEDOT:PSS. (a) and (b) shows the vertical columnar structures deposited at 80^{o} and 25rpm, (c) shows the slanted strutures deposited at 80^{o} with no ratation and (d) shows the dense flat surface.

Figure 4.3 shows the top view SEM images with the contact angle measurement of three samples. Contact angle decreases when surface porosity increases therefore we can see that columnar structures are more hydrophilic than dense films. Flat silicon has 98^{o} while columnar structures possess 71^{o} and 61^{o} contact angle. Also this tests demonstrates that columns lead to enhanced light absorbability and surface interactions.

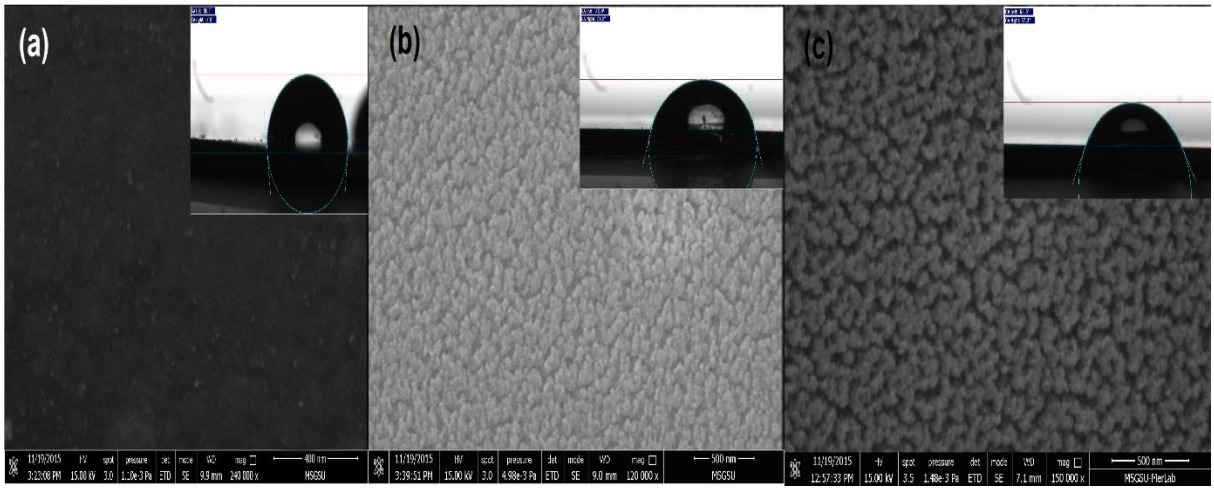

Figure 4.3 : Top-view images and contact angle measurement of (a) flat surface, (b) slanted structure, (c) vertical columnar structure. Surface hyrophilicity increases with the increasing porosity.

Surface porosity also changes optical properties of silicon thin films. Columnar structures possess less reflection compared to the flat surface depending on surface porosity. This phenomena show that we can use these structures as anti-reflection coatings for solar cells and optical devices to decrease reflectivity and increase efficiency. Figure 4.3 shows wavelength-reflectance measurement of 3 samples.

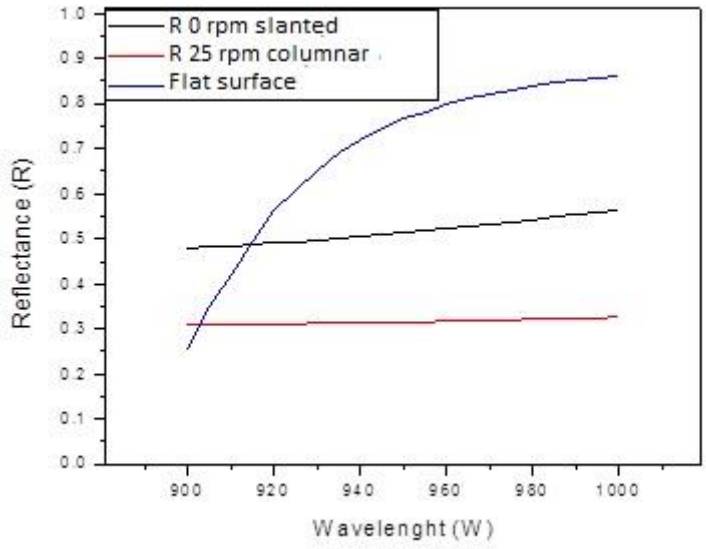

Figure 4.4 : Wavelength-reflectance measurement of flat surface, slanted structures and vertical columnar structures. More porous surface exhibit less reflectance.

Figure 4.4 shows the images of silicon films. Color differences between flat surface and columnar structures of same material can be seen depending on different reflectance.

Figure 4.5 : Color differences of silicon thin films with different geometries. Blue sample on the left is flat surface and yellow samples on the right are columnar structures of 400nm silicon.

Figure 4.6 shows AFM images of flat surface and vertical columnar structures fabricated in 25rpm and 80^{o} in 1μmx1μm area. Columnar structures have higher surface roughness compared to the flat surface. This demonstrates that columnar structures have higher light absorption as well.

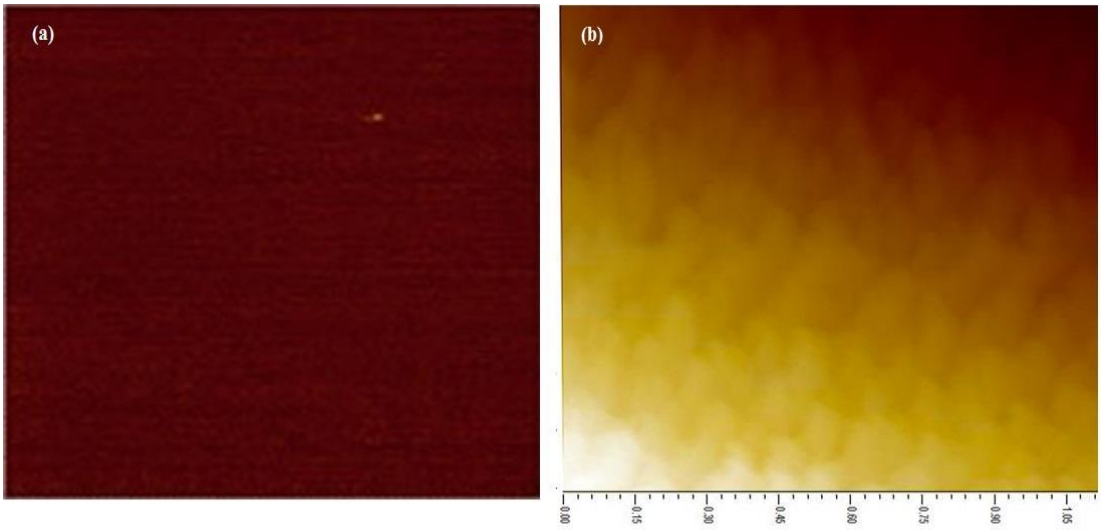

Figure 4.6 : AFM images of (a) flat surface, (b) columnar structures on 1micron area. Columnar structures possess higher surface roughness.

Figure 4.7 shows the XRD measurements of 3 samples. Since amorphous structures were used, no peak was observed.

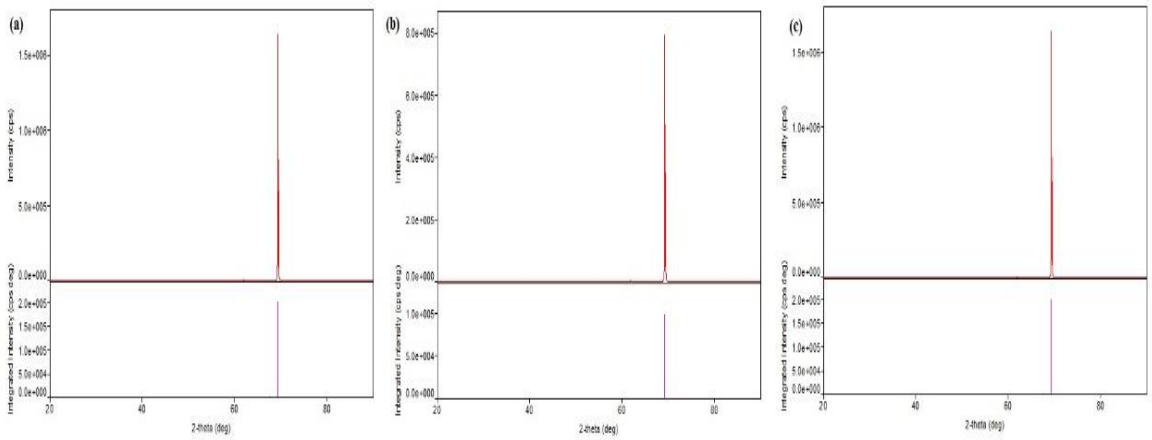

Figure 4.7 : XRD measurements of (a) flat surface, (b) 25rpm vertical columnar structures and (c) slanted clumnar strucutres.

Figure 4.8 shows the transmittance of PEDOT:PSS between the wavelength range of solar radiation inside the atmosphere. This shows the light passes through Ag grid electrode and polymer layer and reaches the silicon absorber layer.

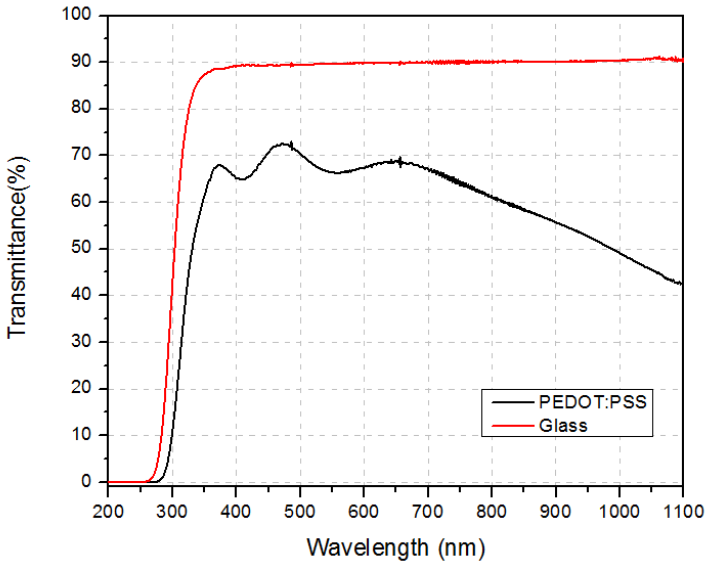

Figure 4.8 : Transmittance measurements of PEDOT:PSS and glass surface. PEDOT exhibit high transperancy.

5. CONCLUSIONS AND RECOMMENDATIONS

In this study nano silicon columnar structures and flat surfaces have been fabricated using glancing angle deposition technique by e-beam evaporation technique. Their important optical, structural and surface parameters investigated that affect photovoltaic properties for solar cell applicaations.

n-Si columnar structures have high porous surfaces that affect optical properties and surface behaviours therefore change the photovoltaic properties.

Both cross-sectional and top-view SEM images shows that columnar structures have higher porosity than flat surfaces.

Columnar structures possess lower reflectance value in UV-VIS spectroscopy which means they have higher absorbance so we can use these structures both for solar cell application and other opto-electronic devices as anti-reflection coating to increase efficiency and other photovoltaic parameters such as fill factor, open circut voltage and short circut current.

Also columnar strucutres have hydrophilic surface due to the high porosity that characteristic eases the distribution of PEDOT:PSS hole conductor polymer on surface and provide better distribution and larger p-n junction interface area.

Since amorphous structures were used in this study no peek was observed in XRD measurement.

PEDOT:PSS was covered on surface using spin coating technique. First it was dropped on surface left for 1 min. then rotated 2000rpm twice to obtain homogenous distribution.

Cross-sectional SEM images shows that columnar structures with PEDOT:PSS have better distribution and larger surface area due to the hydroplicity and porosity while flat surfaces relatively smaller junction area and non-homogenous distribution.

PEDOT:PSS exhibits high transparency in UV-VIS spectroscopy which means light can pass through it and reach the silicon absorber layer to generate electrons and holes.

5.1 What Can Be Done to Increase Efficiency of These Structures?

Columnar structures possess different surface and optical properties than flat surfaces so this effects efficieny of optical devices. Different geometries and shapes can be tried by different kind of methods such as etching and chemical vapor deposition.

For bottom-up methods cooling down the substrate provides better distribution of columnar structure. Since the first impinging atoms are highly energetic, cooler surface reduces the high energy of first arriving atoms and keep them on surface easily.

Nano-crystalline materials can be used instead of amorphous materials to prevent dangling bonds which can cause current leakage. Also surface treatment techniques such as oxidation or hydrogen terminating can be applied to the absorber layer surface.

Quantum dots and carbon nanotubes can be added to silicon absorber layer. Quantum dots have tunable bandgap with changing size that makes them favorable for solar radiation trapping.

Some chemicals (dimethyl sulfoxide, methoxyethanol) can be added to PEDOT:PSS to increase its hole concentration.

REFERENCES

[1] **Sabonnadiere, J. C.** (editor) (2006). *Renewable Energy Technologies.* John Wiley Sons, Inc. ISBN 978-1-84821-135-3.

[2] **Pagliaro M.** (2010). *Nano-Age How Nanotechnology Changes Our Future.* WILEY-VCH. ISBN 975352737676.

[3] **Url-1** < http://www.worldometers.info/ >

[4] **International Energy Agency Energy Statistics.** (2011). *World Energy Statistics 201*.

[5] **Mertens, K**. (2014). *Photovaltaics Fundementals, Technology and Practice Book* John Wiley and Son Ltd. ISBN 9781118634165**.**

[6] **World Energy Consumption Outlook from the International Energy Outlook** Published by DOE Energy Administration.

[7] **International Energy Agency.** (2012). *Key World Energy Statistics 2012,* Retrieved 2012-12-17.

[8] **Url-2** < https://www.euronuclear.org/info/encyclopedia/n/nuclear-power-plant-world-wide.htm >

[9] **Url-3** < https://water.usgs.gov/edu/wuhy.html >

[10] **"Geothermal Capacity About BP Global".** Bp.com. Retrieved 2013-10-05.

[11] **Url-4** < http://instituteforenergyresearch.org/topics/encyclopedia/fossil-fuels/ >

[12] **Url-5** < http://environment.nationalgeographic.com/environment/global-warming/wind-power-profile/ >

[13] **Global Wind Energy Council**. (2014). *Global Wind Statistics.*

[14] **Hovland, K. M.** (2014). Denmark's Wind Power Output Rises to Record in First Half. Wall Street Journal.

[15] **The World Wind Energy Association.** (2014). *Half – year report.*

[16] **Lynn, P. A.** (2010). *Electricity from Sunlight, an Introduction to Photovoltaics*. WILEY. ISBN: 978-0-470-74560-1.

[17] **Schlager, N., Weisblatt, J.** (editors) (2006). *Alternative Energy Volume 2.* THOMSON GALE. ISBN-13: 978-0787694401.

[18] **Url-6** < http://environment.nationalgeographic.com/environment/green-guide/buying-guides/water-heater/shopping-tips/ >

[19] **Url-7** < http://www.samlexsolar.com/learning-center/solar-cell-module-array.aspx >

[20] **Url-8** < http://www.fluor.com/projects/copper-crossing-solar-power-construction >

[21] **Sahu, B. K.** (2015), A study on global solar PV energy developments and policies with special focus on the top ten solar PV power producing countries. *Renewable and Sustainable Energy Reviews*, **43**, 621–634.

[22] **Sarasa-Maestro, C.J., Dufo-López, R., Bernal-Agustín, J.L.** (2013). Photovoltaic remuneration policies in European Union. *Energy Policy*, **55**, 317–28.

[23] **Url-9** < https://www.solarwirtschaft.de/en/media/single-view/news/one-out-of-ten-in-germany-is-already-produc >.

[24] **Url-10** < http://www.inquisitr.com/1982709/germany-builds-a-solar-city-that-produces-four-times-the-energy-it-consumes-video/#utm_content=buffer7b555&utm_medium=social&utm_source=twitter.com&utm_campaign=buffer >.

[25] **Liu L, Wang Z**. (2009). The development and application practice of wind, solar energy, hybrid generation systems in China. *Renewable and Sustainable Energy Reviews,* **13(6),** 1504-1512.

[26] **German Solar Industry Association (BSW-Solar)**. (2012). *Statistic data on the German solar power (photovoltaic)*.

[27] **Jordan – Korte, K.** (2011). *Government Promotion of Renewable Energy Technologies Policy Approaches and Market Development in Germany, the United States and Japan.* Gabler Research. ISBN 978-3-8349-2712-5

[28] **Url-11** < http://www.greentechmedia.com/articles%20/read/u.s.-solar-market-grows-76-in-2012 >.

[29] **Seifried, D. and Witzel, W.** (2010). *Renewable Energy – The Facts.* Routledge. ISBN-13: 978-1849711609.

[30] **Graaf, T. V., Sovacool, B. K.** (2014). Thinking big: Politics, progress, and security in the management of Asian and European energy mega projects. *Energy Policy*, **74**, 16–27.

[31] **Url-12** < http://www.desertec.org/en/press/pictures/ >.

[32] **Vlladen, S.** (2012). PV workshop on theory modeling and simulation. USA: Colorado School of Mines and National Renewable Energy Laboratory. Pardue University.

[33] **Chopra K.L., Paulson P.D., Dutta V.** (2004). Thin – film solar cells: an overview. *Porgress in Photovoltaics,* **12(2-3)**, 69-92.

[34] **Huang, C. H., Chuang, W. J.** (2015). Dependence of performance parameters of CdTe solar cells on semiconductor properties studied by using SCAPS-1D. *Vacuum*, **118**, 32-37.

[35] **Badawy, W. A.** (2015). A review on solar cells from Si-single crystals to porous materials and quantum dots. *Journal of Advanced Research*, **6**, 123–132.

[36] **Url-13** < http://environmentalresearchweb.org/cws/article/news/30489/1/Generationgap >.

[37] **Wright, M., Uddin, A.** (2012). Organic—inorganic hybrid solar cells: A comparative review. *Energy Materials & Solar Cells,* **107**,87–111.

[38] **Technology report by the Fraunhofer Institute for Systems and Innovation Research ISI, Karlsruhe, Germany.** (2013). *Nanotechnology in the sectors of solar energy and energy strorage for IEC market strategy*. Geneva, Switzerland.

[39] **He, L., Jiang, C., Wang, H., Lai, D.** (2011). Simple Approach of Fabricating High Efficiency Si Nanowire/Conductive Polymer Hybrid Solar Cells. *Electron Device Letters, IEEE,* **32(10),** 1406-1408.

[40] **Gea, Z., Xu, L., Zhang, R.** (2015). Improved performance of silicon nanowire/cadmium telluride quantum dots/organic hybrid solar cells. *Applied Surface Science,* **334**, 15–18.

[41] **He, L., Jiang, C., Wang, H., Lai, D.** (2012). High efficiency planar Si/organic heterojunction hybrid solar cells. *Applied Physics Letters*, 100, 073503.

[42] **Tsakalakos L., Balch, J., Fronheiser, J. and Korevaar, B.** (2007). Silicon nanowire solar cells. *Korevaar Applied Physics Letters*, **91**, 233117.

[43] **Brus, V., Zellmeier, M., Zhang, X., Greil, S., Glub M.** (2013). Electrical and photoelectrical properties of P3HT/n-Si hybrid organic–inorganic heterojunction solar cells. *Organic Electronics*, **14**, 3109–3116.

[44] **Shi, E., Zhang, L., Li, Z., Li, P.** (2012). TiO_2-Coated Carbon Nanotube-Silicon Solar Cells with Efficiency of 15%. *Scientific Reports*, 2012.

[45] **Jia Y., Cao A., Bai, X., Li, Z., Zhang L.** (2011). Achieving High Efficiency Silicon-Carbon Nanotube Heterojunction Solar Cells by Acid Doping. *Nano Letters*, **11**, 1901-1905.

[46] **Wang, F. Zhang, X., Wang, L., Fang, J.** (2014). Boron doped nanocrystalline silicon/amorphous silicon hybrid emitter layers used to improve the performance of silicon heterojunction solar cells. *Solar Energy*, **108**, 308–314.

[47] **Karaagac, H., Parlak, M., Yengel, E., Islam, M.S.** (2013). Heterojunction solar cells with integrated Si and ZnO nanowires and a chalcopyrite thin film. *Materials Chemistry and Physics*, **140,** 382-390.

[48] **Tatar, B., Demiroglu, D., Kazmanlı, K., Urgen, M.** (2015). Improvement in electrical and photovoltaic properties of a-Si/c-Si heterojunction with slanted nano-columnar amorphous silicon thin films for photovoltaic applications. *Applied Physics*, **15,** 511-519.

[49] **Goetzberger, A., Knobloch, J. and Vob, B.** (1998). *Crystalline Silicon Solar Cells*, John Wiley & Sons, org. ISBN: 978-0-471-97144-3.

[50] **Laplante, P. A.** (2005). *Comprehensive dictionary for electrical engineering*. CRC Press. ISBN 978-0-8493-3086-5.

[51] **Url-14** < http://www.semiwafer.com/products/silicon.htm >.

[52] **Url-15** < http://www.novawafers.com/resources-about-silicon.html >.

[53] **Url-16** < http://www.primewafers.com/Product_Si.html >.

[54] **Zhang, F., Wenham, S., Green, M.A.** (1995). Large area, concentrator buried contact solar cells. *Electron Devices IEEE Transactions on*, **42(1),** 144-149.

[55] **Soga, T.** (editor) (2006). *Nanostructured Materials for Solar Energy Conversion.* Elsevier, ISBN-13: 978-0444528445.

[56] **Photovoltaics report**. (2014). Fraunhofer ISE,

[57] **Url-17** < https://en.wikipedia.org/wiki/Amorphous_silicon#/media/File:Schematic_of_allotropic_forms_of_silcon_horizontal_plain.svg >.

[58] **Url-18** < http://www.solarproductsstore.com/understanding-solar-equipment/difference-between-monocrystalline-polycrystalline-and-amorphous-thin-film-solar-cell/ >.

[59] **Nagamatsu, K., Avasthi, S., Jhaveri, J., & Sturm, J. C.** (2014). A 12% efficient silicon/PEDOT: PSS heterojunction solar cell fabricated at 100 C. *Photovoltaics, IEEE Journal of*, **4 (1),** 260-264.

[60] **Schmidt, J., Titova, V., & Zielke, D.** (2013). Organic-silicon heterojunction solar cells: Open-circuit voltage potential and stability. *Applied Physics Letters*, **103 (18),** 183901.

[61] **Url-19** < http://www.sigmaaldrich.com/catalog/product/aldrich/483095?lang=en&region=US&gclid=CJe40NCTp8gCFUHnwgodA0UIpQ >.

[62] **Hornyak, G. L., Moore, J. J., Tibbals, H. F., Dutta. J.** (2008). *Fundementals of Nanotechnology*. CRC Press. ISBN 9781420048032.

[63] **Url-20** < http://prof.usb.ve/hreveron/PVD%20pagina.htm >.

[64] **Url-21** < http://www.study-on-line.co.uk/whoami/thesis/chap3.html >

[65] **Robbie, K., Shafai, C., & Brett, M. J.** (1999). Thin films with nanometer-scale pillar microstructure. *Journal of materials research*, **14(07)**, 3158-3163.

[66] **Hawkeye, M., Taschuk, M.T., Brett, M.J.** (2014). *Glancing Angle Deposition of Thin Films: Engineering the Nanoscale*. Matthew WILEY. ISBN: 978-1-118-84756-5.

[67] **Hodkinson, I., Wu, Q.H.** (2001). Inorganic Chiral Optical Materials. *Advanced Materials*, **13,** 889-897.

[68] **Yang, H., Lee, M., Huang, C., Lo, Y., Chen, Y., Wong, M.,** (2009). Glancing angle deposited titania films for dye-sensitized solar cells. *Thin Solid Films*, **518**, 5.

[69] **Dick, B., Brett, M. J., Smy, T. J., Freeman, M. R., Malac, M. Egerton, R. F.,** (2000). Periodic magnetic microstructures by glancing angle deposition. *Journal of Vacuum Science & Technology A*, **18 (4),** 1838-1844.

[70] **Kiema, G. K., Jensen, M. O., Brett, M. J.** (2005). Glancing Angle Deposition Thin Film Microstructures for Microfluidic Applications. *Chemistry of Materials*, **17 (16),** 4046–4048.

[71] **Tyagi, M. Tomar, M., Gupta, V.** (2014). Glad assisted synthesis of NiO nanorods for realization of enzymatic reagentless urea biosensor. *Biosensors and Bioelectronics*, **52,** 196–201.

[72] **Sobahan, K.M.A., Park, Y.J., Hwangbo, C.K.** (2009) Effect of deposition angle on the optical and the structural properties of Ta_2O_5 thin films fabricated by using glancing angle deposition. *Journal of the Korean Physical Society*, **55(3),** 1272-1277.

[73] **Robbies, K., Sit, J. C., Brett, M. J**. (1998). Advanced Techniques for Glancing Angle Deposition. *Journal of Vacuum Science & Technology*, **B 16,** 1115.

[74] **Tait, R.N., Smy, T., Brett, M.J.** (1993). Modelling and characterization of columnar growth in evaporated films. *Thin Solid Films*, **226,** 196-201.

[75] **Messier, R., Gehrke, T., Frankel, C., Venugopal, V. C., Otano, W., Lakhtakia, A.** (1997). Engineered sculptured nematic thin films. J. *Journal of Vacuum Science & Technology*, **A 15**, 2148.

[76] **Zhao, Y., Ye, D., Wang, G. C., & Lu, T. M.** (2003, October). Designing nanostructures by glancing angle deposition. In *Optical Science and Technology, SPIE's 48th Annual Meeting (pp. 59-73).* International Society for Optics and Photonics.

[77] **Url-22** < http://www.brewerscience.com/spin-coating-theory >

CURRICULUM VITAE

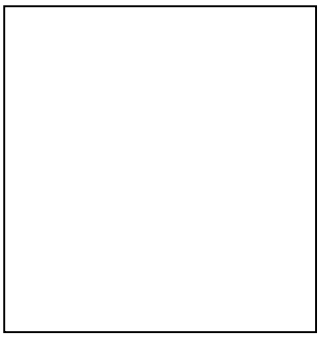

Name-Surname	**:** Ayşegül Develioğlu
Place and Date of Birth	**:** Istanbul, 24.07.1989
E-mail	**:** develioglua@itu.edu.tr
B.Sc. :	**:** 2012, from Gebze Institute of Technology, Physics, Kocaeli/ Turkey.